Development 140, 1055-1066 (2013) doi:10.1242/dev.090860
© 2013. Published by The Company of Biologists Ltd

The transcription factor Otx2 regulates choroid plexus development and function

Pia A. Johansson[1], Martin Irmler[2], Dario Acampora[3,4], Johannes Beckers[2,5], Antonio Simeone[3,4] and Magdalena Götz[1,6,*]

SUMMARY

The choroid plexuses (ChPs) are the main regulators of cerebrospinal fluid (CSF) composition and thereby also control the composition of a principal source of signaling molecules that is in direct contact with neural stem cells in the developing brain. The regulators of ChP development mediating the acquisition of a fate that differs from the neighboring neuroepithelial cells are poorly understood. Here, we demonstrate in mice a crucial role for the transcription factor Otx2 in the development and maintenance of ChP cells. Deletion of *Otx2* by the Otx2-CreERT2 driver line at E9 resulted in a lack of all ChPs, whereas deletion by the Gdf7-Cre driver line affected predominately the hindbrain ChP, which was reduced in size, primarily owing to an increase in apoptosis upon *Otx2* deletion. Strikingly, Otx2 was still required for the maintenance of hindbrain ChP cells at later stages when *Otx2* deletion was induced at E15, demonstrating a central role of Otx2 in ChP development and maintenance. Moreover, the predominant defects in the hindbrain ChP mediated by Gdf7-Cre deletion of *Otx2* revealed its key role in regulating early CSF composition, which was altered in protein content, including the levels of Wnt4 and the Wnt modulator Tgm2. Accordingly, proliferation and Wnt signaling levels were increased in the distant cerebral cortex, suggesting a role of the hindbrain ChP in regulating CSF composition, including key signaling molecules. Thus, Otx2 acts as a master regulator of ChP development, thereby influencing one of the principal sources of signaling in the developing brain, the CSF.

KEY WORDS: Cerebral cortex development, Cerebrospinal fluid, Wnt, Mouse

INTRODUCTION

The local environment, the niche, plays a key role in regulating neural stem and progenitor behavior and identity during development (Johansson et al., 2010). As cerebrospinal fluid (CSF) contains a variety of signaling factors (Parada et al., 2008, Gato and Desmond, 2009; Huang et al., 2010; Johansson et al., 2010; Lehtinen et al., 2011) its composition might contribute to the unique niche environment of the neural stem cells lining the ventricle (Johansson et al., 2010).

In the adult and during development the composition of CSF is predominantly determined by the activities of the four choroid plexuses (ChPs) suspended in the cerebral ventricles (Fig. 1A). The ChPs are formed between embryonic day (E) 11 and 14 in the mouse, with the fourth ventricular (hindbrain) ChP differentiating first followed by the two lateral ventricular and later the third ventricular ChP (Dziegielewska et al., 2001). The ChPs acquire barrier, secretory and transport capacities shortly after formation (Møllgård et al., 1976; Ek et al., 2003; Johansson et al., 2005; Johansson et al., 2006; Liddelow et al., 2009; Ek et al., 2010). This early functionality and their localization inside the cerebral ventricles, together with their appearance during the period of neurogenesis, make them uniquely suited for influencing CSF composition and thereby regulating development of the neural stem cells that are in contact with the ventricle along the entire neuraxis (e.g. Götz and Huttner, 2005). In particular, the fourth ventricular ChP, being the first to appear, might initially regulate the composition of the entire CSF, prior to the appearance of the other ChPs and the start of directed CSF bulk flow and reabsorption.

The role of the ChPs in brain development is still largely unknown, as are the factors that regulate ChP development, although it has been shown that BMP and Notch signaling pathways are initially involved in their development (Hébert et al., 2002; Hunter and Dymecki, 2007; Imayoshi et al., 2008). In the early developing chick embryo, reciprocal inhibition between the neuroepithelial transcription factor Emx2 and Otx2 expressed in the dorsal roof plate plays a role in specifying neuroepithelial versus ChP territories (von Frowein et al., 2006). As Otx2 also acts as a potent fate determinant in other parts of the developing mouse brain (Acampora et al., 1995; Puelles et al., 2004) we set out to elucidate its role in ChP specification and development by genetic deletion of *Otx2* in the mouse brain using the novel Otx2-CreERT2 and the Gdf7-Cre mouse lines. These experiments revealed an absolute requirement of Otx2 in ChP development and a novel role of the ChP as a modulator of Wnt signaling mediated via the CSF.

MATERIALS AND METHODS

Animals

All animals were kept in the animal facility of the Helmholtz Center Munich. The day of the vaginal plug was counted as E0. The developmental age was confirmed by measurements of crown-rump length. All experimental procedures were performed in accordance with German and European Union guidelines. The following mouse lines were used: *Otx2* floxed (Puelles et al., 2003), Gdf7-Cre (Lee et al., 2000), TG(Fos-lacZ)34Efu/J Wnt reporter (DasGupta and Fuchs, 1999) and CAG-GFP reporter (Nakamura et al., 2006). We also created a novel mouse line, Otx2-CreERT2 (supplementary material Fig. S1), by replacing the genomic

[1]Helmholtz Center Munich, German Research Center for Environmental Health, Institute for Stem Cell Research, Neuherberg, 85764 Munich, Germany. [2]Helmholtz Center Munich, German Research Center for Environmental Health, Institute for Experimental Genetics, Neuherberg, 85764 Munich, Germany. [3]Institute of Genetics and Biophysics, A. Buzzati-Traverso, CNR Via P. Castellino 111, 80131 Naples, Italy. [4]IRCCS Neuromed, 86077 Pozzilli (IS), Italy. [5]Technical University Munich, Center of Life and Food Sciences Weihenstephan, 85354 Freising, Germany. [6]Physiological Genomics, University of Munich, 80336 Munich, Germany.

*Author for correspondence (magdalena.goetz@helmholtz-muenchen.de)

Accepted 19 December 2012

region spanning the entire *Otx2* coding sequence with the tamoxifen-inducible CreERT2 recombinase followed by the *Otx2* 3′UTR and polyadenylation signal (Feil et al., 1997). The Otx2-CreERT2 mice were treated with 0.1 mg/g body weight tamoxifen (Sigma) in order to induce recombination. Tamoxifen was dissolved in corn oil and administered once to the pregnant mother via oral gavage.

Tissue processing

Whole heads and bodies (E11-13) and brains [E14, E20 and postnatal day (P) 2] were fixed by immersion in 4% (w/v) paraformaldehyde in phosphate-buffered saline (PBS). P7 brains were first perfused with the same fixative followed by immersion. The heads and brains were washed in PBS and immersed in 30% sucrose (w/v in PBS). The tissue was then embedded in Tissue-Tek OCT Compound and frozen on dry ice and cut (cryostat, 12-20 μm) and stored at −20°C.

Immunohistochemistry

Frozen sections were thawed and washed in PBS followed by blocking solution (0.5% Triton X-100, 10% normal goat serum in PBS). The sections were incubated in primary antibodies: rabbit anti-Otx2 (1:200, Chemicon), goat anti-Otx2 (1:600, R&D Systems), chick anti-GFP (1:1000, Aves), rabbit anti-phospho-histone H3 (PH3, 1:400, Millipore), rabbit anti-Pax6 (1:500, Chemicon), rat anti-Pecam/CD31 (Pecam1 – Mouse Genome Informatics) (1:30, BD Pharmingen), rat anti-prominin 1 (1:500, eBiosciences), rabbit anti-cyclin D1 (1:20, Thermoscientific), rabbit anti-β-galactosidase (1:5000, MP Biologicals), rabbit anti-Tbr1 (1:200, Abcam), rat anti-Ctip2 (Bcl11b – Mouse Genome Informatics) (1:200, Abcam) and rabbit anti-Cux1 (1:200, Santa Cruz). The sections were washed in PBS and incubated with secondary antibodies (Alexa 488 or 546 conjugated, Jackson Laboratories). Nuclei were visualized by DAPI. Sections were analyzed using an Olympus Axioplan2 confocal laser-scanning microscope.

In situ hybridization

In situ hybridization was performed on frozen tissue (tissue preparation as for immunohistochemistry) with digoxigenin (DIG)-labeled riboprobes (Roche) according to standard procedures. Probes were made by cloning of gene-specific PCR products into the StrataClone PCR Cloning Vector using the StrataClone PCR Cloning Kit and subsequent sequencing: *Wnt5a* (1026 bp, nucleotides 629-1635 in NM_009524), *Ttr* (600 bp, 14-614 in NM_013697), *Ngn2* (*Neurog2* – Mouse Genome Informatics) (741 bp, 896-1637 in NM_009718), *Hes5* (1196 bp, 75-1291 in NM_010419).

FACS analysis for cell death (annexin V assay)

E13 hindbrain ChP or cerebral cortices were dissected and dissociated to a single-cell suspension by 15 minute incubation in 0.05% trypsin followed by mechanical dissociation. In cases of co-analysis with prominin 1, the cells were incubated with FITC-conjugated prominin 1 antibody (CD133, eBioscience). Cell death was assessed using the PI/APC-conjugated Annexin V Kit (eBioscience) followed by FACS analysis (FACSAria, BD Biosciences). Gating parameters were determined by side and forward scatter to eliminate debris (P1 gate) and aggregated cells (P2 gate). Non-stained controls were used to set the gates for PI and annexin V (annexin A5 – Mouse Genome Informatics) (set to include no more than 0.1% of non-fluorescent cells). A FITC-conjugated isotype control (eBioscience) was used to set the prominin 1 gate (set to exclude the majority of the cells; see supplementary material Fig. S3). A total of 5000 or 30,000 cells were included in each ChP or cerebral cortex analysis, respectively.

CSF sampling and analysis

Samples of CSF were collected from the fourth ventricle using microcapillary samplers (E12-14, typically 0.5-2 μl) (see Johansson et al., 2006). All CSF samples were microscopically examined for traces of blood over a white background and samples that showed any sign of blood contamination were discarded. The samples were stored at −20°C until analyzed. Total protein concentration was measured using the standard Bradford assay.

Primary cortical cultures

The brains of E13 wild-type embryos were dissected out and the meninges removed. The cerebral cortices were isolated from the rest of the brain and dissociated as previously described (Costa et al., 2008) and cultured in poly-D-lysine-coated 96-well plates (80,000 cells/well) in DMEM-GlutaMAX (Invitrogen) containing CSF (10 or 15%) without further media changes or growth factor additions. After 72 hours the number of cells was assessed using the MTS colorimetric proliferation assay (CellTiter 96 AQueous One Solution Cell Proliferation Assay, Promega). Each sample (n=3 for each condition) contained CSF from six to ten embryos from two to three litters.

Wnt (β-galactosidase) reporter gene assay

Canonical Wnt signaling activity was monitored using the β-Gal Reporter Gene Assay (Roche). Cerebral cortices (pooled from two embryos for each sample) and rostral spinal cords were isolated from E13 *Otx2*$^{fl/fl}$ and *Gdf7-Cre*/*Otx2*$^{fl/fl}$ embryos also carrying the TOPGAL reporter gene (Jackson Laboratories). The chemiluminescence emitted from the deglycosylation of the substrate Galacton Plus was measured using the Orion II Microplate Luminometer (Berthold Detection Systems). Serial dilutions of the β-galactosidase positive control (provided with the kit) were included in the experiments and the concentration of β-galactosidase in each sample was derived from the standard curve.

Transcriptome analysis

Hindbrain ChP was microdissected at E13 from *Gdf7-Cre*/*Otx2*$^{fl/fl}$ and control animals (four pooled samples per genotype, each pooled sample containing two to four ChPs). Total RNA was isolated using the RNeasy Micro Kit (Qiagen) including digestion of remaining genomic DNA. The Agilent 2100 Bioanalyzer was used to assess RNA quality and only high-quality RNA (RIN >8) was used for microarray analysis. Total RNA (80 ng) was amplified using the one-cycle MessageAmp Premier Labeling Kit (Ambion) and 10 μg amplified RNA was hybridized on Affymetrix Mouse Genome 430 2.0 arrays containing ~45,000 probe sets. Staining and scanning were performed according to the Affymetrix expression protocol. Heat maps were generated with CARMAweb and dendrograms with R (hclust) (Rainer et al., 2006). Gene ontology term and pathway enrichment analyses were performed with GePS software (Genomatix, Germany). Secreted proteins were determined with GePS software and manual curation. Array data are available at GEO under accession number GSE27630.

RNA isolation, cDNA synthesis and real-time PCR analysis

Total RNA from microdissected E13 hindbrain ChPs (three to four, pooled), E14-15 lateral ventricular ChPs (one to three, pooled), E13 cerebral cortices (midline excluded, two brains pooled per sample) or E13 rostral spinal cords (two cords pooled per sample) was extracted using the RNeasy Micro Kit (Qiagen) for ChP or the RNeasy Mini Kit (Qiagen) for cortex and spinal cord. RNA was reversed transcribed into cDNA using random primers and Superscript III First-Strand Synthesis SuperMix (Invitrogen). The real-time RT-PCR assay was conducted using SYBR Green Dye Master Mix (Bio-Rad). Primer sets for all genes (supplementary material Table S5) were validated using melting curve analysis and gel electrophoresis. Assays were performed in triplicate on a DNA Engine Opticon machine (Bio-Rad). The relative expression of each mRNA was calculated between the gene of interest and *Gapdh* using the formula $E=2^{-(-\Delta\Delta Ct)}$, and normalized to the expression levels in the control.

Western blot

CSF from E13 *Otx2*$^{fl/fl}$ and *Gdf7-Cre*/*Otx2*$^{fl/fl}$ embryos was sampled as described above. The same volume of CSF was loaded onto each well (12% Tris-HCl gels) and separated by electrophoresis (Mini-PROTEAN 3 Cell System, Bio-Rad). The proteins were transferred onto a PVDF membrane (Millipore) by wet transfer, followed by blocking in Tris-buffered saline containing 5% skimmed milk and then primary antibody incubation in rabbit anti-Tgm2 (1:250, Zedeira) or rabbit anti-Wnt4 (1:500, Abcam), followed by an HRP-conjugated secondary antibody (1:30,000, GE Healthcare). The signal was detected using Immobilon Western Chemiluminescent HRP High-Sensitivity Substrate (Millipore) and X-ray film exposure. Developed X-ray films were digitalized using the CanoScan N670U (Canon) and Adobe Photoshop CS3.

Statistical analysis

Statistical analysis of the microarrays was performed utilizing the statistical programming environment R (R Development Core Team, 2005) implemented in CARMAweb (Rainer et al., 2006). Briefly, probe set summaries were calculated with RMA (R-based Microarray Analysis; default settings including quantile normalization and application of Tukey's median polish algorithm) and genewise testing for differential expression was performed employing the limma *t*-test and Benjamini-Hochberg multiple testing correction [false discovery rate (FDR) <10%].

All other results were analyzed using the unpaired or paired two-tailed Student's *t*-test. The normal distribution of the mutant phenotype was analyzed using the Kolmogorov-Smirnov test for the FACS analysis data (largest dataset) and were found to fit to a normal distribution ($P>0.05$). In all tests, $P<0.05$ was considered statistically significant. All error bars indicate s.e.m.

RESULTS

Otx2 is required for the development of all ChP epithelial cells

In order to study the role of Otx2 in ChP development we generated a new mouse line expressing the tamoxifen-inducible form of Cre (Otx2-CreERT2; supplementary material Fig. S1) in the *Otx2* locus, and mated this with $Otx2^{fl/fl}$ mice in order to conditionally delete *Otx2* upon tamoxifen administration. Tamoxifen (0.1 mg/g body weight) was given to mothers that were pregnant for 9 days, and recombination was monitored in GFP reporter (CAG-GFP) mice (Nakamura et al., 2006). GFP protein was widespread in the dorsal midline at E11 throughout the brain (Fig. 1B,C; supplementary material Fig. S1) and Otx2 protein levels were already reduced in lateral ventricular ChP anlage at E11 (Fig. 1D,E). Transthyretin (*Ttr*) expression was also reduced only 2 days after initiation of recombination at this age (Fig. 1F,G). At E12, the *Ttr*-expressing domain was virtually absent in the rostral part of the lateral ventricular ChP and the third ventricular ChP anlage (Fig. 1H,M). The cortical hem, as visualized by the *Wnt5a*-expressing domain, appeared unaffected at E12, indicating a ChP-specific effect (Fig. 1N,O). Strikingly, at E13, when the lateral and fourth ventricular ChPs are normally both differentiated and invaginated into the ventricle (Fig. 1P,S,U), all four ChPs in the forebrain (including the third ventricular ChP anlage) and hindbrain were virtually absent in the mutant brains (Fig. 1Q,R,T,V; data not shown). In some cases, a small ChP remnant was found caudally, but this was not *Ttr* positive (Fig. 1W,X). Analysis using *Wnt5a*

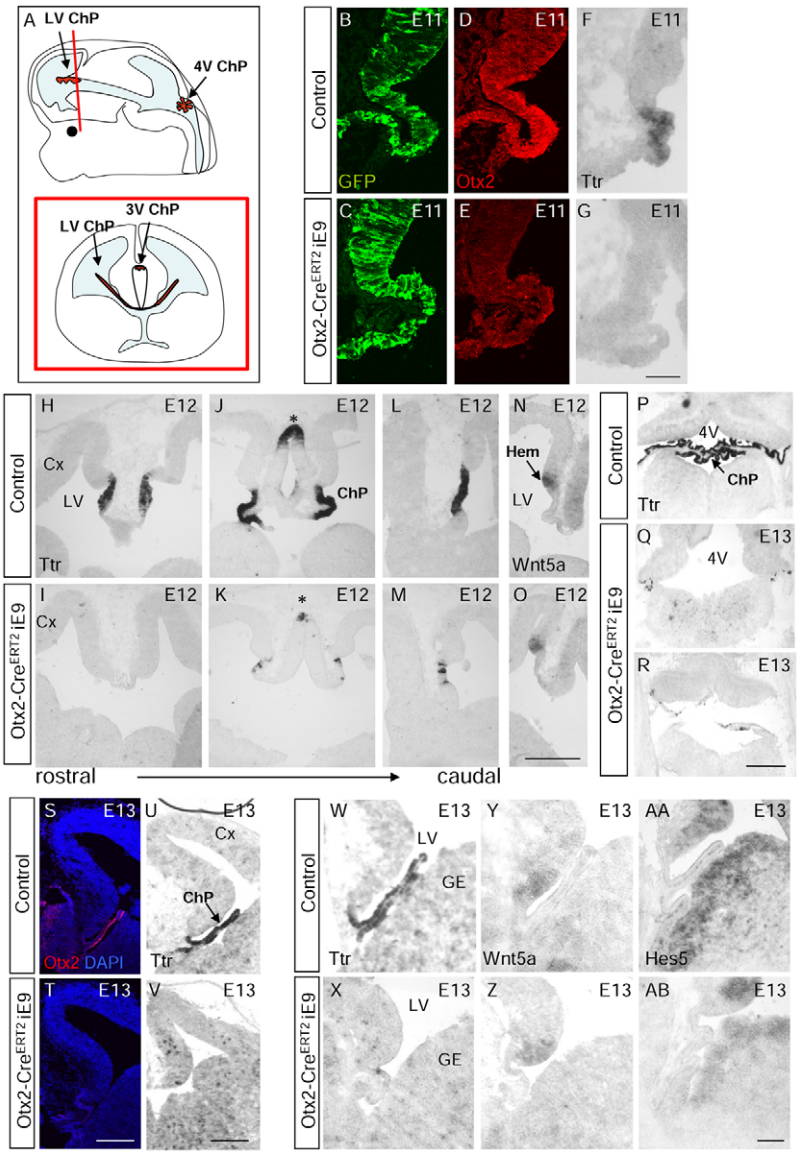

Fig. 1. *Otx2* deletion using Otx2-CreERT2 and E9 induction results in the absence of all four ChPs. (**A**) Schematic showing the localization of all four ChPs in the mouse embryonic brain. The third ventricular ChP is situated between the two lateral ventricular ChPs; they cannot be visualized in the same sagittal representation, and thus a coronal depiction of the forebrain (beneath) shows the localization of the third ventricular ChP and its relation to the two lateral ventricular ChPs. The red line in the sagittal depiction indicates the level of the coronal depiction. (**B-G**) Micrographs of coronal sections of E11 control (*Otx2-CreERT2/CAG-GFP*) and *Otx2-CreERT2/*$Otx2^{fl/fl}$*/CAG-GFP* mice after E9 tamoxifen induction showing recombination in the dorsal midline (B,C; GFP immunohistochemistry) and decrease in Otx2 (D,E; immunohistochemistry) and *Ttr* (F,G; *in situ* hybridization). (**H-O**) Micrographs of coronal sections of E12 control and *Otx2-CreERT2/*$Otx2^{fl/fl}$ mice after E9 tamoxifen induction. *Ttr* (H-M) and *Wnt5a* (N,O) *in situ* hybridization show the virtual absence of all four ChPs but an intact cortical hem territory (M,N). Asterisk indicates the third ventricular ChP. (**P-AB**) Micrographs of coronal sections of E13 control (*Otx2-CreERT2* or $Otx2^{fl/+}$) and *Otx2-CreERT2/*$Otx2^{fl/fl}$ mice after E9-10 tamoxifen induction. (P-R) *Ttr in situ* hybridization shows the absence of the hindbrain ChP after *Otx2* deletion (Q,R). (S,T) Sections stained with an antibody against Otx2. *Ttr in situ* hybridization (U,V) shows the absence of specified ChP territory in rostral sections. *In situ* hybridization for *Ttr* (W,X), *Wnt5a* (Y,Z) and *Hes5* (AA,AB) at more caudal regions of the forebrain show that the former ChP territory remained unspecified. LV, lateral ventricle; 3V, third ventricle; 4V, fourth ventricle; ChP, choroid plexus; Cx, cerebral cortex; GE, ganglionic eminence. Scale bars: 50 μm in B-G; 250 μm in H-O; 100 μm in P-AB.

(Fig. 1Y,Z) and *Hes5* (Fig. 1AA,AB) showed that the hem or neuroepithelial domains were not extended into the ChP domain; instead, a small *Ttr*-negative domain remained at the site of the ChP. Thus, deletion of *Otx2* by Otx2-CreERT2 revealed a key role of Otx2 in the development of all ChPs, resulting in the ultimate disappearance of virtually all ChP cells.

To determine whether Otx2 is also required for the maintenance of the ChP after specification, we induced recombination at E15 in the Otx2-CreERT2 mice (Fig. 2). Five days after induction, Otx2 was no longer detectable in most ChP cells of all four ChPs (Fig. 2A,B; data not shown), with the exception of a very few epithelial cells still being positive (arrow in Fig. 2B); however, the ChP epithelial cells and the entire ChP structures appeared unaltered in size. At 10 days after induction (P7), the size of the lateral and third ventricular ChPs appeared unaffected (Fig. 2C,D; data not shown). However, the fourth ventricular ChP was much smaller (a decrease in rostrocaudal expansion rather than in lateral to medial length; Fig. 2E,F), suggesting a continued, but less acute, role for Otx2 in maintenance of the hindbrain ChP. The reduced size of the fourth ventricular ChP was evident at both medial and lateral levels (sagittal sections) as well as by microscopic inspection of the whole brain. This suggested a region-specific role for Otx2 in ChP maintenance, which is in contrast to the uniform requirement for Otx2 in early ChP development.

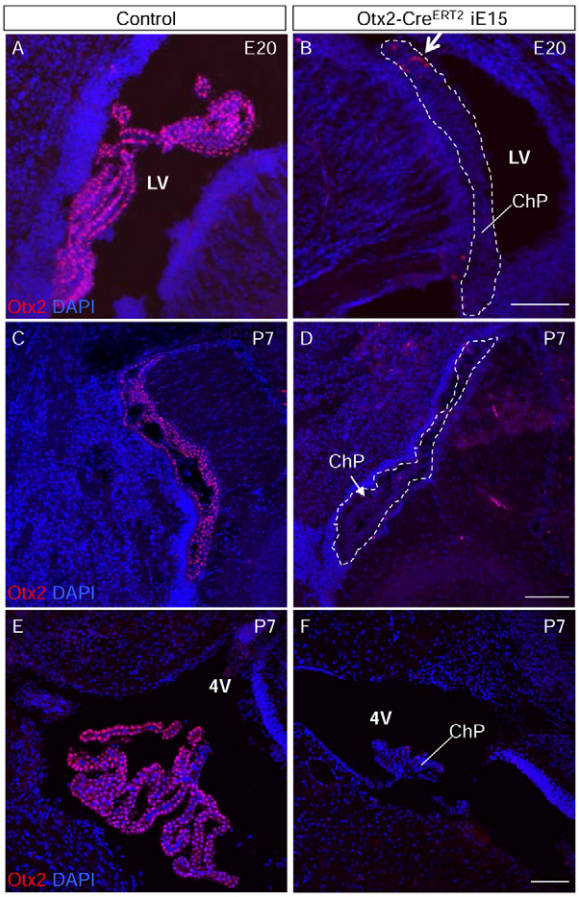

Fig. 2. *Otx2* deletion using Otx2-CreERT2 and E15 induction results in region-specific effects on the ChPs. (**A**,**B**) Confocal images of coronal sections of forebrain immunostained for Otx2 (red) in control and *Otx2-CreERT2/Otx2*$^{fl/fl}$ E20 mice after E15 tamoxifen induction showing the normal appearance of the ChPs despite the absence of Otx2. Note the occasional remaining Otx2^{+} cell (arrow). (**C-F**) Confocal images of sagittal sections immunostained for Otx2 in control and *Otx2-CreERT2/Otx2*$^{fl/fl}$ P7 mice after E15 tamoxifen induction showing normal sized lateral ChPs (D, outlined with dashed lines) but a smaller hindbrain ChP (F). LV, lateral ventricle; 4V, fourth ventricle. Scale bars: 100 μm.

Otx2 is required for the survival of cells in the hindbrain ChP

Although the above data suggest a key role of Otx2 in ChP development, CreERT2-mediated deletion is not specific to the roof plate and ChP regions, but also occurs in the ventral telencephalon, midbrain and various other regions of the brain expressing Otx2 (supplementary material Fig. S1). We therefore searched for a more ChP-specific Cre driver. As recombination in the Gdf7-Cre mouse line has previously been shown to be specific to the roof plate and to occur in the cells generating the hindbrain ChP (Lee et al., 2000; Currle et al., 2005), we examined Gdf7-Cre-mediated recombination in the *Otx2*$^{fl/+}$ background. We observed recombination in the hindbrain ChP, in the dorsal midline of the midbrain and the diencephalon (supplementary material Fig. S2), and very little recombination in the lateral ventricular ChP (in only a few cells in a restricted number of sections of the ChP; supplementary material Fig. S2). We also saw reporter gene expression in what appeared to be the telencephalic meninges, as well as in scattered cells in the hind- and midbrain areas (supplementary material Fig S2).

Consistent with the virtual absence of recombination in the lateral ventricular ChPs, all DAPI-labeled epithelial cells were still Otx2 immunopositive from E13 to E16 (Fig. 3A-D), the *Otx2* mRNA levels were comparable (Fig. 3E) and no significant defects in size or maturation of the lateral ventricular ChPs in *Gdf7-Cre*/*Otx2*$^{fl/fl}$ mice or controls (*Gdf7-Cre*/*Otx2*$^{fl/+}$ or *Otx2*$^{fl/fl}$) were detectable (Fig. 3F-J). The nearby cortical hem also appeared normal (Fig. 3K,L). Likewise, the third ventricular ChP also appeared normal (Fig. 3G-J) despite higher levels of reporter gene activity in this region (supplementary material Fig. S2). Conversely, we observed a dramatic decrease in the size of the hindbrain ChP by E13 (Fig. 4C,D), but not yet consistently so at E12 (Fig. 4A,B). The reduction in size was seen in all *Gdf7-Cre*/*Otx2*$^{fl/fl}$ embryos in all coronal sections containing hindbrain ChP, and was not due to Cre toxicity as the heterozygous embryos (*Gdf7-Cre*/*Otx2*$^{fl/+}$) did not exhibit this phenotype. Accordingly, *Otx2* mRNA levels as measured by real-time RT-PCR were significantly decreased in hindbrain ChP tissue isolated from E13 *Gdf7-Cre*/*Otx2*$^{fl/fl}$ versus control embryos (Fig. 4E).

Analysis of serial sections of the ChP revealed that the recombination efficiency was not complete at all levels, as visualized by the absence of GFP reporter in some fourth ventricular ChP epithelial cells (Fig. 4F; compare also with supplementary material Fig. S2L). Notably, many of the ChP cells remaining at E13 (Fig. 4G) were not reporter positive, suggesting that some epithelial cells escape the *Otx2* deletion and thus the E13 ChPs in *Otx2*$^{fl/fl}$ mice mostly consist of non-recombined Otx2^{+} cells. The concept of 'escaping' epithelial cells was verified by the presence of a smaller Otx2^{+} hindbrain ChP remaining at lateral levels at P2 (Fig. 4H,I) and in the adult (data not shown). The presence of a much smaller ChP at P2 and adult stages also indicated the absence of compensatory growth or regrowth of the ChP. Thus, Gdf7-Cre-mediated *Otx2* deletion results in a significant reduction in the size of the hindbrain ChP, while not evidently affecting the ChP of the lateral and third ventricles.

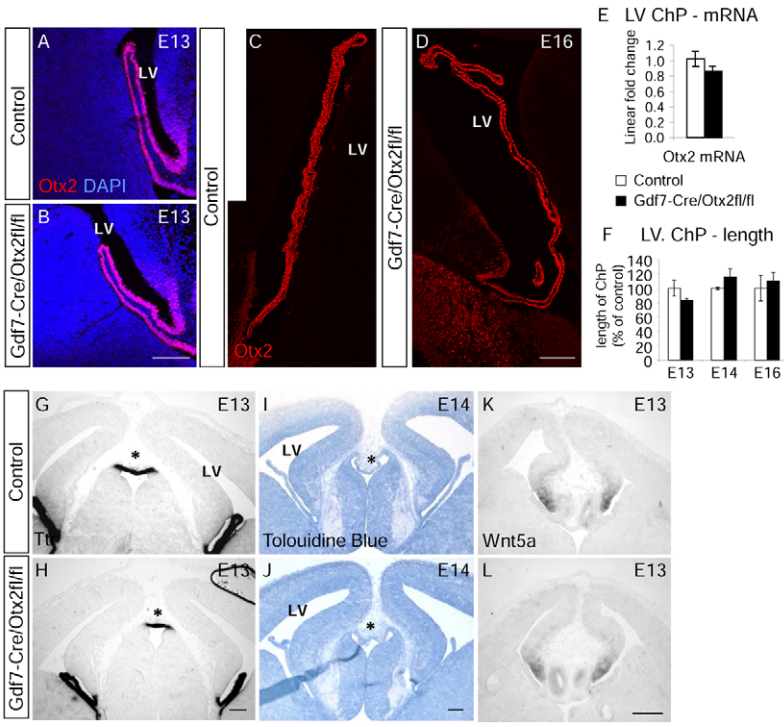

Fig. 3. The forebrain ChPs remain unaffected in *Gdf7-Cre/Otx2*$^{fl/fl}$ mice. (**A-D**) Confocal image stacks of coronal sections of forebrain ChP from E13 (A,B) and E16 (C,D) control and *Gdf7-Cre/Otx2*$^{fl/fl}$ embryos immunostained for Otx2 (red), with nuclei labeled with DAPI (blue). (**E**) Relative *Otx2* mRNA levels in isolated E14/15 lateral ventricular ChP. (**F**) Relative length of the lateral ventricular ChP at E13-16. Error bars indicate s.e.m. (**G-L**) Micrographs showing *Ttr in situ* hybridization (G,H), Tolouidine Blue staining (I,J) and Wnt5a *in situ* hybridization (K,L) in coronal sections of forebrain ChPs from E13 control and *Gdf7-Cre/Otx2*$^{fl/fl}$ embryos. Asterisk indicates the third ventricular ChP. LV, lateral ventricle. Scale bars: 100 μm.

To evaluate the possibility of increased cell death as a cause for the size reduction observed in the *Gdf7-Cre/Otx2*$^{fl/fl}$ hindbrain ChP, we used fluorescence-activated cell sorting (FACS) of annexin V and propidium iodide (PI) (Fig. 5A,B; supplementary material Fig. S3). This revealed a significant increase in both late (PI$^+$/annexin V$^+$, 2.4-fold increase) and early (annexin V$^+$, 2.1-fold increase) apoptosis among cells isolated from the E13 *Gdf7-Cre/Otx2*$^{fl/fl}$ hindbrain ChP compared with controls (Fig. 5B). The percentage of necrotic cells (PI only; Fig. 5B) was low in all samples and not significantly altered in the mutant. To assess the levels of apoptosis specifically in the ChP epithelial cells, we used double labeling with an antibody recognizing prominin 1 (CD133) localized on the ChP epithelial cells (Fig. 5C). As expected, prominin 1$^+$ epithelial cells from the mutant *Gdf7-Cre/Otx2*$^{fl/fl}$ ChP showed an increase in apoptosis (late and early apoptosis combined, 2.5-fold increase; Fig. 5D), suggesting that ChP epithelial cells enter the apoptosis pathway upon deletion of *Otx2*.

The reduced ChP size and increased cell death might be due to aberrant proliferation. Staining for the phosphorylated form of histone H3 (PH3) that is present in late G2/M phase of the cell cycle revealed a significant reduction of PH3$^+$ cells in the hindbrain ChP of *Gdf7-Cre/Otx2*$^{fl/fl}$ compared with control embryos [Fig. 5E-G; the proliferative zone belonging to the ChP is delineated by the absence of Pax6 (Landsberg et al., 2005)], suggesting that reduced proliferation might further contribute to the decreased size of the *Gdf7-Cre/Otx2*$^{fl/fl}$ hindbrain ChP at this age.

Given the signaling between the ChP epithelial and endothelial cells (Wilting and Christ, 1989; Nielsen and Dymecki, 2010), we also examined blood vessels by PECAM immunohistochemistry. The blood vessels formed at normal density in the *Gdf7-Cre/Otx2*$^{fl/fl}$ hindbrain ChP region, even though they appeared somewhat more disorganized (supplementary material Fig. S3). Thus, various defects occur after Otx2 protein loss at ~E13 in the hindbrain ChP, the most prominent of which is pronounced cell death.

Changes in CSF composition after deletion of *Otx2* in the hindbrain ChP

As the hindbrain ChP develops first and is the largest at E13, we hypothesized that its severe reduction might affect CSF composition. Total protein concentration was determined in CSF collected from control and *Gdf7-Cre/Otx2*$^{fl/fl}$ embryos using the standard Bradford assay. This analysis revealed a significant increase in CSF protein concentration in the *Gdf7-Cre/Otx2*$^{fl/fl}$ mice at E13 and E14 (30% and 60% increases over control values, respectively) but not at E12 (Fig. 6A).

In order to assess whether the altered composition of CSF from mutant embryos had any functional consequences (and to examine the extent to which an *in vivo* phenotype could be due purely to altered intraventricular pressure resulting from the smaller ChP), CSF from control and *Gdf7-Cre/Otx2*$^{fl/fl}$ mice was sampled from the fourth ventricle (E13) and added to primary dissociated cerebral cortex cultures from E13 wild-type mice (Costa et al., 2008). The cells were grown for 3 days in DMEM-GlutaMAX and 10% CSF from either genotype (with no additional growth factors or mitogens). Interestingly, the number of cells, as shown by the MTS assay, was significantly increased when CSF from *Gdf7-Cre/Otx2*$^{fl/fl}$ mice was added as compared with CSF from control mice (35% increase; Fig. 6B). This was not due to a global increase in CSF protein, as the addition of more control CSF (15%) did not alter cell numbers. Thus, depletion of hindbrain ChP by Gdf7-Cre-mediated *Otx2* deletion affects CSF composition.

Transcriptome analysis of hindbrain ChP reveals major alterations in the expression of secreted signaling factors in *Gdf7-Cre/Otx2*$^{fl/fl}$ embryos

Given the above results we next set out to determine the factors that are altered in the *Gdf7-Cre/Otx2*$^{fl/fl}$ CSF, supposedly based on altered expression/release from the hindbrain ChP. Genome-wide expression analysis of microdissected control (*Otx2*$^{fl/fl}$) and mutant hindbrain ChP was performed using Affymetrix MOE430 2.0

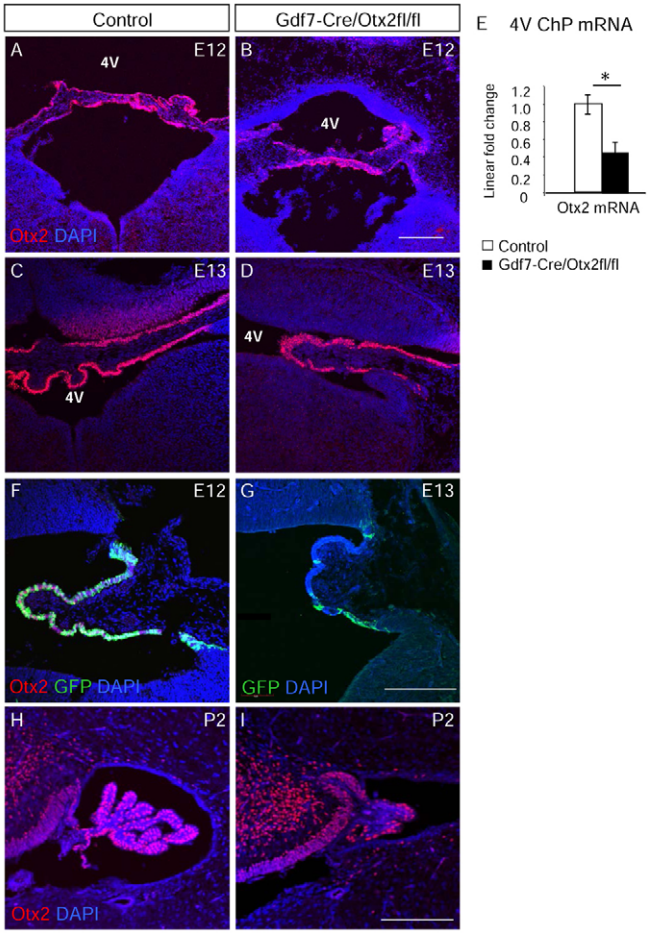

Fig. 4. *Otx2* deletion using the Gdf7-Cre mouse line results in a smaller hindbrain ChP. (**A-D**) Confocal image stacks of coronal sections of the hindbrain ChP from E12-13 control and *Gdf7-Cre/Otx2*$^{fl/fl}$ mice immunostained for Otx2 (red). (**E**) Relative *Otx2* mRNA levels in isolated E13 hindbrain ChP. *P<0.05; error bars indicate s.e.m. (**F**,**G**) Confocal image stacks of coronal sections of the hindbrain ChP from P2 control and *Gdf7-Cre/Otx2*$^{fl/fl}$ mice immunostained for Otx2 and GFP. (**H**,**I**) Confocal image stacks of coronal sections of the hindbrain ChP from *Gdf7-Cre/CAG-GFP* and *Gdf7-Cre/Otx2*$^{fl/fl}$*/CAG-GFP* mice immunostained for Otx2 and GFP. 4V, fourth ventricle. Scale bars: 200 μm.

arrays. Clustering of the array data (supplementary material Fig. S4) grouped the samples according to their genotype. Reassuringly, genes already known to be highly expressed in the ChP, such as the very abundant *Ttr*, Igf and *Aqp1* mRNAs (Lehtinen et al., 2011; Marques et al., 2011), were also highly expressed in the current analysis. Indeed, *Ttr* is the second most abundant mRNA in E13 control ChP and is similarly abundant in the mutant ChP, suggesting that our dissection procedure was successful in isolating the remnant ChP and that no major change in composition of the ChP was evident.

The transcriptome analysis revealed 511 significantly (FDR<10%) differentially expressed probe sets, which had expression levels exceeding 50 in at least one group and linear ratios that exceeded 2-fold (supplementary material Fig. S4). In total, 192 probe sets were upregulated (corresponding to 135 genes) and 319 downregulated (corresponding to 225 genes) (supplementary material Tables S1, S2). In order to validate the differences in gene expression as predicted by the microarray analysis, ten genes (chosen for their biological significance as well as to represent a range of fold changes and expression levels) were investigated by real-time RT-PCR (on the same RNA used for the arrays as well as on independent samples). The up- or downregulation of all selected genes was confirmed, and nine out of ten RT-PCR results were significant (P<0.05; supplementary material Fig. S4).

We then focused specifically on genes encoding diffusible factors (supplementary material Tables S3, S4) and noted several components of the Wnt signaling pathway with significantly altered expression in the *Gdf7-Cre/Otx2*$^{fl/fl}$ hindbrain ChP (Table 1). The upregulation of *Rspo1*, *Wnt4*, *Sfrp2* and *Tgm2*, as well as the downregulation of *Sostdc1*, would all point to increased Wnt signaling mediated via the CSF. Conversely, no changes were observed in the expression of Igf and related factors previously suggested to play important roles in signaling via the CSF (Huang et al., 2010; Lehtinen et al., 2011).

In order to directly measure some of the Wnt signaling modulators that display altered expression in the mutant hindbrain ChP, CSF was sampled from several embryos, pooled as one biological replicate and equal volumes of control and mutant CSF were loaded onto single lanes on a western blot (n=3 biological replicates). Remarkably, Wnt4 and Tgm2 were not only detectable in the CSF collected from control embryos (Fig. 6C), but both also showed a considerable increase in concentration in the CSF from *Gdf7-Cre/Otx2*$^{fl/fl}$ embryos (Fig. 6C), thereby confirming that the gene expression changes observed in the mutant hindbrain ChP are reflected at the protein level in the CSF.

Altered proliferation and Wnt signaling in the cerebral cortex

As the above data suggest that the deletion of the *Otx2*$^{-/-}$ hindbrain ChP affects CSF composition, including modulators of the Wnt pathway, we examined the extent to which this affects the neuroepithelial cells lining the ventricle. As Wnt signaling would affect proliferation, we examined PH3 in three different regions of the *Gdf7-Cre/Otx2*$^{fl/fl}$ mice, namely the cerebral cortex, the lateral ganglionic eminence (LGE) and the spinal cord, all of which are in contact with CSF. Even though Gdf7-Cre-driven recombination did not affect the forebrain (see also supplementary material Fig. S2), we found an increase in apical (ventricle-contacting) PH3$^+$ cells per hemisphere (30% increase; Fig. 7A-C; see also supplementary material Fig. S5), whereas PH3$^+$ basal progenitors were slightly reduced (by 10%) in number (Fig. 7A-C) in the cerebral cortex of *Gdf7-Cre/Otx2*$^{fl/fl}$ E13 embryos. These data are consistent with the role of Wnt signaling in promoting stem cell self-renewal, causing a decrease in the generation of intermediate neuronal progenitors dividing basally. This effect appeared to be surprisingly specific to the dorsal telencephalon as no changes in proliferation were observed in either the LGE of the ventral telencephalon or in the spinal cord (Fig. 7D,E; supplementary material Fig. S5).

As the smaller hindbrain ChP was primarily caused by an increase in apoptosis, and as diffusible and secreted factors regulating apoptosis could reach the cerebral cortex via the CSF, we also investigated cell death in the cerebral cortex at E13 by FACS analysis of annexin V as described above (Fig. 7F). No changes in apoptosis were seen in the radial glia (prominin 1$^+$ cells), whereas a decrease (by 25%) in apoptosis was seen in the prominin 1$^-$ population (basal progenitors and neurons). This decrease could potentially explain the decrease in PH3$^+$ basal progenitors, but not the increase in PH3$^+$ apical progenitors, consistent with the increase in apical progenitors being caused by increased Wnt signaling from the CSF.

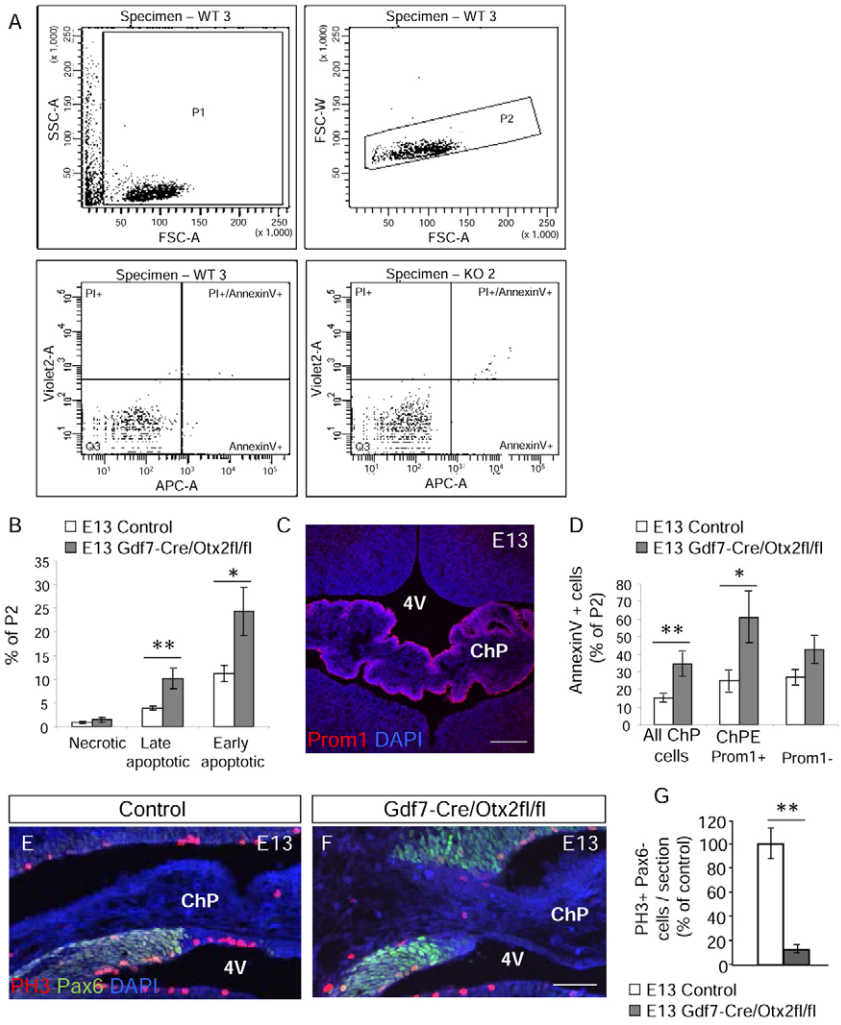

Fig. 5. The reduced size of the hindbrain ChP after *Otx2* deletion using the Gdf7-Cre mouse line results mainly from an increase in apoptosis. (**A**) FACS setup showing P1 and P2 gates (far left and left) and the selection of cells for analysis and example blots (right and far right) from one control (WT 3) and one mutant (KO 2) analysis. (**B**) Quantification of the FACS analysis. (**C**) Micrograph depicting prominin 1 immunostaining in the epithelial cells of control hindbrain ChP at E13. Nuclei are labeled with DAPI. (**D**) Quantification of the prominin 1 co-analysis; n=6-8. (**E**,**F**) Micrographs of coronal sections depicting proliferating cells of the hindbrain ChP labeled by phospho-histone H3 (PH3) antibody and absence of Pax6. (**G**) Quantification of $PH3^+$ cells in the hindbrain ChP; n=3. *P<0.05, **P<0.01; error bars indicate s.e.m. ChPE, ChP epithelial cells; 4V, fourth ventricle. Scale bars: 100 µm in C; 40 µm in E,F.

To determine which signaling pathways might be involved in the alterations in proliferation, we used real-time RT-PCR to determine the expression of genes considered to be direct target genes of particular signaling pathways. This analysis, of RNA isolated from the cerebral cortices, revealed significant changes in the expression of target genes associated with Wnt signaling and proliferation (cyclin D1, upregulated) as well as the Notch signaling pathway (*Hes1* and *Ngn2*, downregulated), but no changes in target genes associated with the Shh, Fgf or Tgfβ signaling pathways (supplementary material Fig. S6).

To directly monitor canonical Wnt signaling in tissues in contact with the altered CSF, we crossed *Gdf7-Cre*/*Otx2*$^{fl/fl}$ mice with the TOPGAL (TG) reporter mice carrying a β-galactosidase reporter driven by several TCF/Lef binding sites (DasGupta and Fuchs, 1999). We then investigated whether Wnt reporter localization (Fig. 7G,H) or levels (Fig. 7I) were altered in the embryos with a mutant hindbrain ChP. The localization of β-galactosidase (as visualized by immunohistochemistry) was unchanged in the *Gdf7-Cre*/*Otx2*$^{fl/fl}$/*TG* mice, with no apparent ectopic Wnt activity in the neuronal population, nor was there a spreading of the hippocampal anlage into the cortex proper, suggesting no change in this aspect of neocortical patterning. However, quantification of the levels of β-galactosidase using a chemiluminescent assay revealed a significant increase (by 30%; Fig. 7I) in E13 cerebral cortices from mutant (*Gdf7-Cre*/*Otx2*$^{fl/fl}$/*TG*) compared with control (*Otx2*$^{fl/fl}$/*TG*) mice, with no significant changes in the spinal cord (data not shown). Thus, region-specific alterations in canonical Wnt signaling correspond to the region-specific changes in proliferation and modulation of Wnt signaling components in the CSF.

Long-term effects of transient alterations in cortical Wnt signaling

Next, we investigated how the alterations in the cerebral cortex would further develop. Interestingly, the increase in proliferation observed at E13 had reversed at E16, when we found a decrease in $PH3^+$ cells at the apical surface (40% decrease; Fig. 8A). This alteration in the proliferation phenotype could be explained by an intrinsic compensatory effect in the progenitor cells with regard to proliferation and/or apoptosis (e.g. Ciaroni et al., 1995), by differences in Wnt signaling (levels and response) at later stages of embryonic development (Chenn, 2008; Pöschl et al., 2012), or could be due to the alterations in CSF composition, which are now greatly modulated by the large and phenotypically normal lateral ventricular ChP reducing the influence of the hindbrain ChP. In accordance with the two latter options, the increased levels of Wnt signaling found at E13 were no longer detectable at E16 (Fig. 8B), suggesting that the changes seen earlier were transient.

We then investigated the long-term effects of this transient increase in Wnt signaling by immunohistochemical analysis of the cerebral cortex at P7 (Fig. 8C). Although no gross defects were

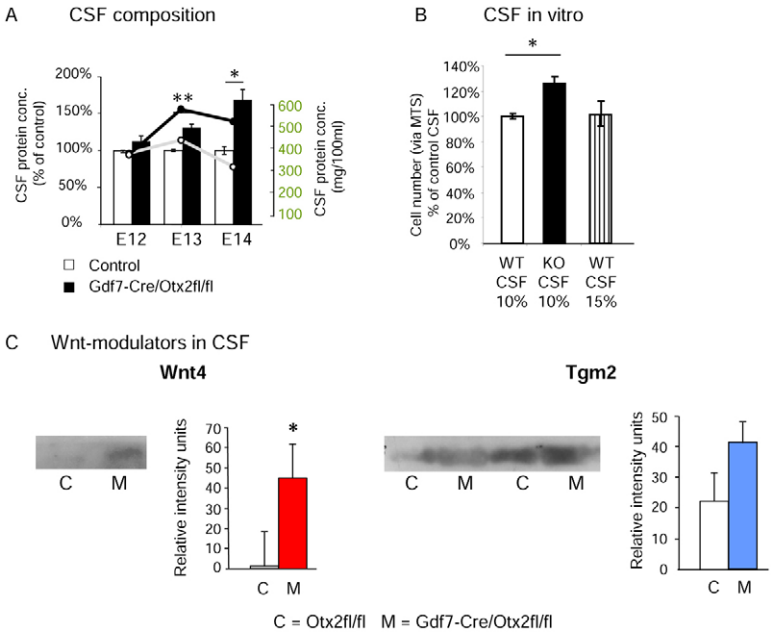

Fig. 6. The smaller hindbrain ChP after *Otx2* deletion using the Gdf7-Cre mouse line alters CSF composition. (**A**) Relative and total protein concentrations in CSF sampled from the fourth ventricle. A significant increase in protein levels was seen in CSF from *Gdf7-Cre/Otx2*$^{fl/fl}$ mice at E13 and E14; *n*=4-6. (**B**) An increase in the number of cortical cells after 3 days in culture with media supplemented with CSF from E13 *Gdf7-Cre/Otx2*$^{fl/fl}$ versus control embryos; *n*=3. (**C**) Western blot analysis of Wnt4 and Tgm2 concentration in CSF from E13 control and *Gdf7-Cre/Otx2*$^{fl/fl}$ embryos. Equal volumes of CSF were loaded onto the gel and their relative concentration analyzed, showing increased concentrations of both Wnt4 and Tgm2 in CSF from the mutant embryos. **P*<0.05, ***P*<0.01; for the Tgm2 analysis *P*=0.09; error bars indicate s.e.m.

detected at this stage, histological analysis revealed a region-specific reduction (by 20%) in layer 5 neurons (detected as Ctip2^{+}/Tbr1^{-} cells; Fig. 8D-I). As these neurons are largely produced at the time when we observe an increase in proliferation, this phenotype is consistent with the progenitor cells remaining longer in the cell cycle rather than exiting to differentiate into neurons. Conversely, layers containing neurons generated earlier or later were not significantly altered in their thickness.

DISCUSSION

Otx2 as a master regulator of ChP development and maintenance

Here we demonstrated a key role for Otx2 in ChP development by deletion of *Otx2* at three different time points during development using two distinct Cre lines. Deletion of *Otx2* during the initial stages of development affects ChP development rapidly and profoundly. Upon deletion of *Otx2* by induction of recombination at E9 and complete absence of Otx2-immunopositive cells by E11, all ChPs failed to form. Notably, this was a ChP-specific effect, as another roof plate-derived structure that also expresses Otx2, the nearby cortical hem, was unaffected. Thus, whereas Otx2 is not vital for the hem, it is absolutely required for all four ChPs, with very little remnant structures at E12/13 in the absence of Otx2. The vast majority of ChP cells are either not specified or die at such an early state in their differentiation that they cannot be distinguished. Notably, a very small remnant structure (estimated at 1-2% of control ChP size) of the lateral ChP remains as a single layer of non-pseudostratified epithelium that is clearly distinct from the adjacent neuroepithelium but still largely fails to differentiate ChP hallmarks such as Ttr expression.

A similarly profound role for Otx2 was seen at later stages when using the Gdf7-Cre driver (onset of protein loss at E11/12), with only Otx2^{+} cells – either escapers from recombination (GFP reporter negative/Otx2^{+}) or in the process of losing Otx2 (GFP^{+}/Otx2^{+}; reduced *Otx2* mRNA levels at E13 suggest ongoing loss of Otx2) – surviving and forming the ChP remnants. When Otx2 protein is lost at these slightly later stages ChP cells still succumb immediately to cell death, as they are unable to survive without sufficient levels of Otx2.

These data revealed Otx2 as a master regulator of ChP development, it being absolutely essential for these structures to appear. Strikingly, this essential role remains when Otx2 protein is deleted at E20 and the hindbrain ChP subsequently decreases significantly in size. As less proliferation occurs at this time, this effect is also likely to be due to many ChP cells undergoing cell death. Interestingly, in other systems loss of Otx2 also leads to an increase in apoptosis, such as in the adult mouse retinal pigment epithelium and photoreceptors and in GnRH neurons (Béby et al., 2010; Diaczok et al., 2011). These results imply a role for Otx2 as a key regulator of genes that are essential for the function and identity of these cells, such that they fail to survive without them, or the direct regulation by Otx2 of anti-apoptotic genes. The latter function has recently been demonstrated for a variety of homeobox and paired-type homeobox transcription factors (Ninkovic et al., 2010; Fuchs et al., 2012; Moon et al., 2012).

A further exciting and entirely unexpected result is the region-specific effect of Otx2 in ChP maintenance, as observed upon Otx2-CreERT2 line induction at E15. Whereas the hindbrain ChP was severely reduced in size by P7, this was not obvious for the other ChPs, suggesting – to our knowledge for the first time – region-

Table 1. Microarray data for genes with significantly altered expression in *Gdf7-Cre/Otx2*$^{fl/fl}$ hindbrain ChP that encode diffusible components of Wnt signaling

Gene	Ratio*	KO‡	WT‡	Documented effect on Wnt signaling
Wif1	2.6	312	118	Decrease
Rspo1	3.0	481	161	Increase
Wnt4	2.1	737	356	Increase
Sfrp2	2.1	1420	692	Decrease or increase
Dkk2	6.9	2214	322	Decrease or increase
Tgm2	2.0	480	236	Increase
Sostdc1 (*Wise*)	0.4	1808	4209	Decrease

*Linear ratio of *Otx2* knockout/control.
‡Average expression level in *Otx2* knockout (KO) or wild type (WT).

DEVELOPMENT

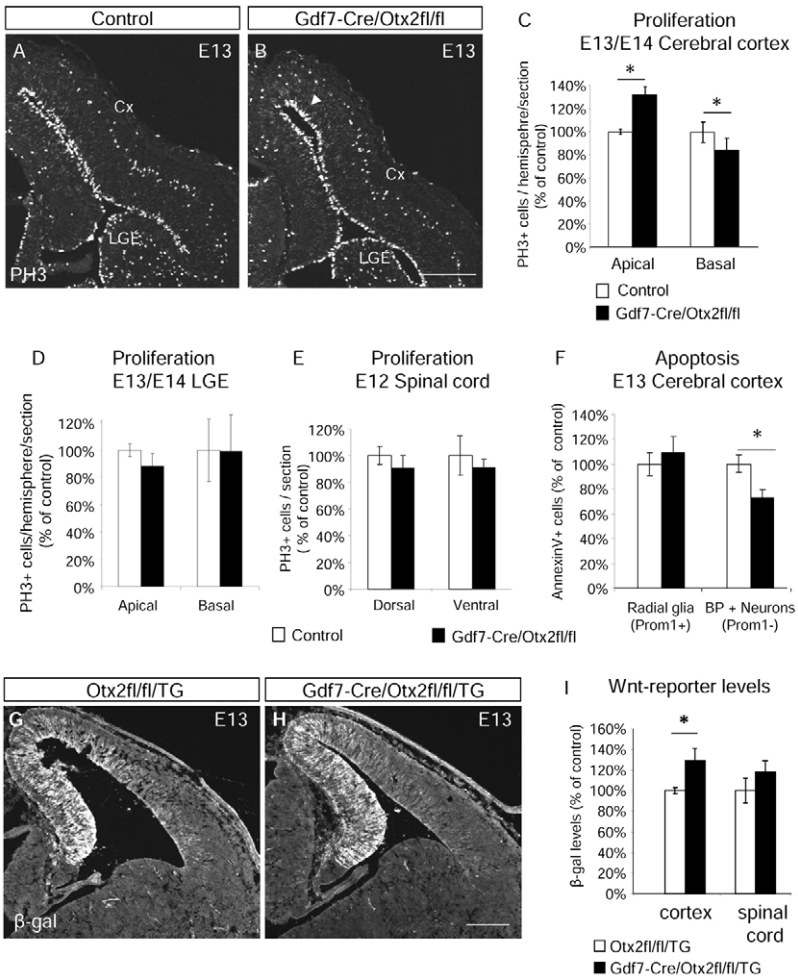

Fig. 7. Changes in cerebral cortex proliferation and Wnt signaling after deletion of *Otx2* in the hindbrain ChP using Gdf7-Cre. (**A**,**B**) Micrographs of coronal sections of forebrain immunostained for PH3. Note the increase in the number of apically proliferating cells in the cerebral cortex (Cx) (arrowhead) in the *Gdf7-Cre/Otx2*$^{fl/fl}$ mice. (**C-E**) Quantification of PH3^{+} cells in cortex (C), lateral ganglionic eminence (LGE) (D) and spinal cord (E). PH3 quantifications showed a significant increase in apically dividing cells in the cerebral cortex and a significant decrease in basally dividing cells at E13/E14. *n*=5. (**F**) Levels of apoptosis (FACS analysis of annexin V) in E13 cerebral cortex showing no change in radial glia (prominin 1^{+} cells) but a small decrease in apoptosis in prominin 1^{-} cells [basal progenitors (BP) and neurons]. *n*=5. (**G**,**H**) Micrographs of coronal sections of forebrain from control (*Otx2*$^{fl/fl}$*/TG*; C) and *Gdf7-Cre/Otx2*$^{fl/fl}$*/TG* (D) embryos immunostained for β-galactosidase. No change in the localization of the Wnt reporter was observed. (**I**) Quantification of Wnt signaling in control (*Otx2*$^{fl/fl}$*/TG*) and *Gdf7-Cre/Otx2*$^{fl/fl}$*/TG* cortices and spinal cords, showing a significant increase in Wnt signaling in the cerebral cortices from embryos with a mutant hindbrain ChP. *n*=5. *P<0.05; error bars indicate s.e.m. Scale bars: 200 μm.

specific differences between the ChPs at this stage. It is now of importance to unravel the region-specific differences in ChPs at the molecular and cellular levels. In this regard, it is of interest that we detected an increase in Wnt signaling components and modulators in the CSF when the hindbrain ChP was most affected by earlier *Otx2* deletion, whereas other signaling molecules in the CSF, such as Shh (Huang et al., 2010) and Igf (Lehtinen et al., 2011), were not altered in their expression levels in the mutant hindbrain ChP. Thus, our work revealing the key role of Otx2 in ChP development now opens novel avenues to further our understanding of these key structures in the developing brain.

Wnt-mediated signaling via the CSF

In addition to revealing Otx2 as a novel key regulator of ChP development, our data are also consistent with a new role for the hindbrain ChP in long-distance signaling mediated by members and modulators of the Wnt signaling pathway (see supplementary material Fig. S7). In the present study, we found that Gdf7-Cre-mediated deletion of *Otx2* leads to changes in CSF composition that affect the proliferation of cells from the cerebral cortex *in vitro* and *in vivo*. CSF sampled from *Gdf7-Cre*/*Otx2*$^{fl/fl}$ mice and administered to cell cultures of cerebral cortex progenitors resulted in increased cell numbers, consistent with the increased proliferation of cells in this region of the mutant embryos. Moreover, based on a transcriptome analysis of the mutant hindbrain ChP that revealed increased expression of Wnt4 and Tgm2, a positive modulator of Wnt signaling (Beazley et al., 2012), we also detected increased levels of these proteins in the CSF of *Gdf7-Cre*/*Otx2*$^{fl/fl}$ mice compared with that collected from control littermates. We then showed that the activity of a TCF/Lef reporter is increased in the cerebral cortex, but not the spinal cord, in the mutant mice, consistent with increased proliferation in the region with increased levels of Wnt signaling. Moreover, the region-specific effects demonstrate that despite the ubiquitous contact of neuroepithelial cells with the CSF, their intrinsic competence regulates their response, as cells in the LGE and spinal cord did not exhibit altered proliferation or Wnt signaling. Thus, our work unraveled a novel route of Wnt signaling from the hindbrain ChP via the CSF.

Interestingly, Otx2 has previously been shown to regulate Wnt ligands, directly or indirectly, along with other signaling molecules in various tissues during development; for example, Wnt ligands and Nodal in the anterior visceral endoderm (Perea-Gomez et al., 2001) and Wnt1, Fgf8 and Shh in the mid/hindbrain region (Acampora et al., 1997; Puelles et al., 2003; Prakash et al., 2006; Omodei et al., 2008). These data prompt the suggestion that Otx2 might commonly affect targets of the Wnt pathway in various cell types, with distinct effects depending on the region and developmental stage. Moreover, Otx2-deficient hindbrain ChP was also altered in the expression of other diffusible signaling molecules, such as members and modulators of the Fgf and Tgfβ families, supporting Otx2 as a key regulator of non-cell-autonomous signaling in development.

However, it is important to bear in mind that the gene expression changes observed in our study might not be solely due to a direct

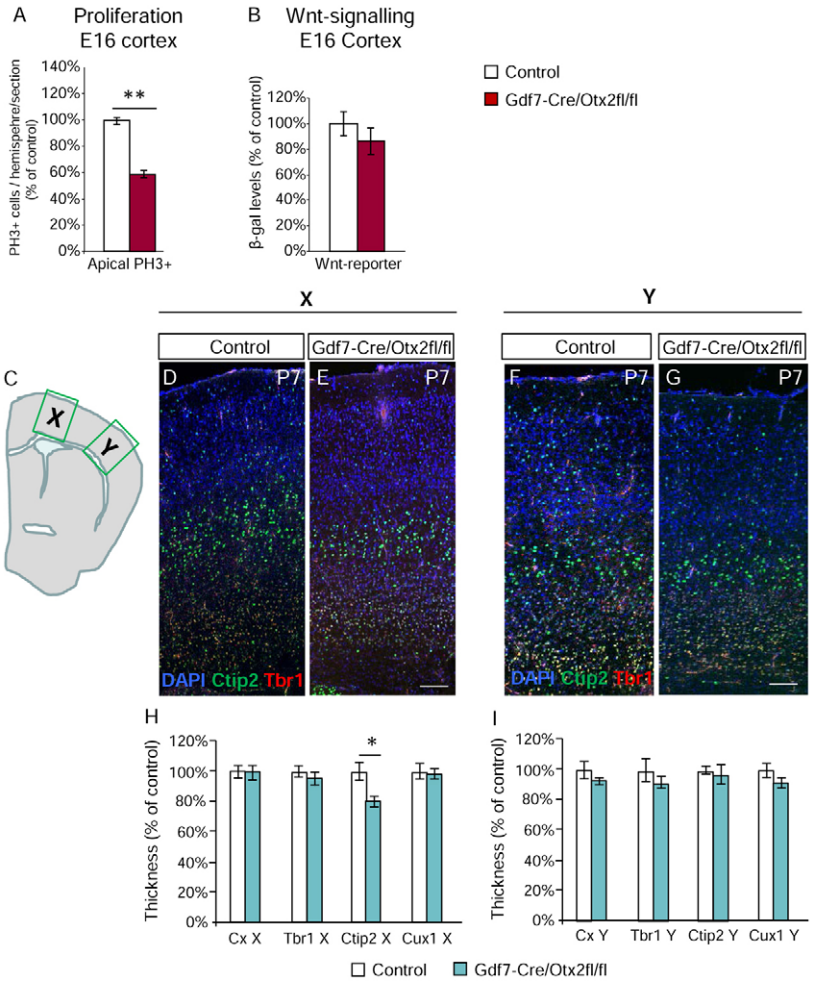

Fig. 8. Changes in mouse cerebral cortex development at E16 and P7 after deletion of *Otx2* in the hindbrain ChP using Gdf7-Cre. (**A**,**B**) Quantification of the percentage of apical PH3$^+$ cells (A) and β-galactosidase levels (B) in E16 control and *Gdf7-Cre/Otx2*$^{fl/fl}$ cortices, showing a decrease in proliferation. *n*=3-5. (C-I) P7 analysis. (**C**) Schematic of the approximate rostrocaudal level and areas (X and Y) analyzed. (**D-G**) Micrographs of coronal sections of forebrain immunostained for Tbr1 and Ctip2 from control (*Otx2*$^{fl/fl}$; D,F) and *Gdf7-Cre/Otx2*$^{fl/fl}$ (E,G) pups. (**H**,**I**) Quantification of cortical and cortical layer thickness in area X (H) and Y (I). *n*=4-5. **P*<0.05, ***P*<0.01; error bars indicate s.e.m. Scale bars: 100 μm.

effect of Otx2 loss, as a change in composition of the ChP itself (e.g. the ratio of epithelial cells to stroma) and other secondary effects due to the induction of apoptosis might well contribute to changes in expression levels. Notably, the Otx2 protein itself is also secreted (Sugiyama et al., 2008) and might hence be present in different amounts in the CSF from *Gdf7-Cre/Otx2*$^{fl/fl}$ embryos compared with control embryos. However, no Otx2 protein was detectable in the ventricular zone of the cerebral cortex, which does not express *Otx2* mRNA, suggesting that the amount of Otx2 protein taken up by these cells is, if at all, rather low under control conditions.

Interestingly, the changes in CSF composition in the *Gdf7-Cre/Otx2*$^{fl/fl}$ embryos appear to be largely mediated by the defects in the hindbrain ChP, as no defects were detectable in the ChPs of the lateral and third ventricle. This would suggest that most, if not all, of the phenotypic abnormalities observed in the cerebral cortex (increased Wnt signaling and proliferation) should be caused by impaired development and functioning of the hindbrain ChP. This hypothesis is further supported experimentally by the observation that CSF sampled from the fourth ventricle of *Gdf7-Cre/Otx2*$^{fl/fl}$ mutant mice affects cerebral cortex progenitors *in vitro* in a way that strongly resembles the phenotype observed *in vivo*. Moreover, changes in mRNA levels in the hindbrain ChP and in the CSF concentration of positive Wnt regulators fit with a major role of the hindbrain ChP in mediating these changes.

However, we noted that recombination mediated via Gdf7-Cre also occurs in the midbrain roof plate, which expresses Otx2 and is in contact with the CSF, suggesting that these cells might contribute to the observed changes in CSF composition, even if they are not visibly defective in their development. Also, if other regions contribute to this phenotype, this work highlights the key roles of ChP differentiation in signaling during brain development beyond neighboring regions (Huang et al., 2010). Given the profoundly altered expression levels of Wnt4 and other modulators of Wnt signaling in the hindbrain ChP upon Gdf7-Cre-mediated *Otx2* deletion, we suggest that this ChP at least contributes to the alterations in Wnt signaling in the distant cerebral cortex via changes in CSF composition. This supports the hypothesis of a modulatory fine-tuning effect mediated by the CSF.

Consistent with the modest change in Wnt signaling and proliferation (with regard to both timing and magnitude) we detected a small region- and layer-specific change in neuronal number as a consequence of manipulation of the hindbrain ChP. Interestingly, changes in neuron numbers in specific layers of the cerebral cortex occur in a region-specific manner during phylogeny and ontogeny, in order to achieve the area-specific tasks that differ profoundly in various mammalian species (Molnár et al., 2006; Krubitzer, 2007). Thus, fine-tuning neuron numbers in a region- and layer-specific manner is functionally relevant, as also shown by experimental manipulation (Pinto et al., 2009). Our data raise the exciting prospect that long-distance signaling via ChP takes part in such processes during ontogeny and phylogeny by modulating stem cell proliferation at specific times in specific brain regions.

Acknowledgements
We thank Tom Jessell and Kevin Lee for the generous gift of the Gdf7-Cre mice; Andrea Steiner, Angelika Waiser, Detlef Franzen, Julia Niewand and Timucin Öztürk for technical support; and the animal caretakers of the Helmholtz Center Munich for their assistance.

Funding
This work was supported by the Humboldt Foundation Research Fellowship (P.A.J. is a Fellow); the German Research Foundation (DFG); the FP6 Project for the European Transcriptome, Regulome and Cellular Commitment Consortium (EuTRACC) Integrated Project [LSHG-CT-2007-037445] and the Italian Association for Cancer Research (AIRC) [IG 5499]; and in part by the Helmholtz Alliance CoReNe to J.B. and M.G.

Competing interests statement
The authors declare no competing financial interests.

Supplementary material
Supplementary material available online at
http://dev.biologists.org/lookup/suppl/doi:10.1242/dev.090860/-/DC1

References

Acampora, D., Mazan, S., Lallemand, Y., Avantaggiato, V., Maury, M., Simeone, A. and Brûlet, P. (1995). Forebrain and midbrain regions are deleted in Otx2-/- mutants due to a defective anterior neuroectoderm specification during gastrulation. *Development* **121**, 3279-3290.
Acampora, D., Avantaggiato, V., Tuorto, F. and Simeone, A. (1997). Genetic control of brain morphogenesis through Otx gene dosage requirement. *Development* **124**, 3639-3650.
Beazley, K. E., Deasey, S., Lima, F. and Nurminskaya, M. V. (2012). Transglutaminase 2-mediated activation of β-catenin signaling has a critical role in warfarin-induced vascular calcification. *Arterioscler. Thromb. Vasc. Biol.* **32**, 123-130.
Béby, F., Housset, M., Fossat, N., Le Greneur, C., Flamant, F., Godement, P. and Lamonerie, T. (2010). Otx2 gene deletion in adult mouse retina induces rapid RPE dystrophy and slow photoreceptor degeneration. *PLoS ONE* **5**, e11673.
Chenn, A. (2008). Wnt/beta-catenin signaling in cerebral cortical development. *Organogenesis* **4**, 76-80.
Ciaroni, S., Cecchini, T., Ambrogini, P., Buffi, O. and Del Grande, P. (1995). Cell death and cell number in the developing cerebral cortex of MAM treated mice. *J. Hirnforsch.* **36**, 161-170.
Costa, M. R., Wen, G., Lepier, A., Schroeder, T. and Götz, M. (2008). Par-complex proteins promote proliferative progenitor divisions in the developing mouse cerebral cortex. *Development* **135**, 11-22.
Currle, D. S., Cheng, X., Hsu, C. M. and Monuki, E. S. (2005). Direct and indirect roles of CNS dorsal midline cells in choroid plexus epithelia formation. *Development* **132**, 3549-3559.
DasGupta, R. and Fuchs, E. (1999). Multiple roles for activated LEF/TCF transcription complexes during hair follicle development and differentiation. *Development* **126**, 4557-4568.
Diaczok, D., DiVall, S., Matsuo, I., Wondisford, F. E., Wolfe, A. M. and Radovick, S. (2011). Deletion of Otx2 in GnRH neurons results in a mouse model of hypogonadotropic hypogonadism. *Mol. Endocrinol.* **25**, 833-846.
Dziegielewska, K. M., Ek, J., Habgood, M. D. and Saunders, N. R. (2001). Development of the choroid plexus. *Microsc. Res. Tech.* **52**, 5-20.
Ek, C. J., Habgood, M. D., Dziegielewska, K. M. and Saunders, N. R. (2003). Structural characteristics and barrier properties of the choroid plexuses in developing brain of the opossum (Monodelphis Domestica). *J. Comp. Neurol.* **460**, 451-464.
Ek, C. J., Wong, A., Liddelow, S. A., Johansson, P. A., Dziegielewska, K. M. and Saunders, N. R. (2010). Efflux mechanisms at the developing brain barriers: ABC-transporters in the fetal and postnatal rat. *Toxicol. Lett.* **197**, 51-59.
Feil, R., Wagner, J., Metzger, D. and Chambon, P. (1997). Regulation of Cre recombinase activity by mutated estrogen receptor ligand-binding domains. *Biochem. Biophys. Res. Commun.* **237**, 752-757.
Fuchs, J., Stettler, O., Alvarez-Fischer, D., Prochiantz, A., Moya, K. L. and Joshi, R. L. (2012). Engrailed signaling in axon guidance and neuron survival. *Eur. J. Neurosci.* **35**, 1837-1845.
Gato, A. and Desmond, M. E. (2009). Why the embryo still matters: CSF and the neuroepithelium as interdependent regulators of embryonic brain growth, morphogenesis and histiogenesis. *Dev. Biol.* **327**, 263-272.
Götz, M. and Huttner, W. B. (2005). The cell biology of neurogenesis. *Nat. Rev. Mol. Cell Biol.* **6**, 777-788.
Hébert, J. M., Mishina, Y. and McConnell, S. K. (2002). BMP signaling is required locally to pattern the dorsal telencephalic midline. *Neuron* **35**, 1029-1041.
Huang, X., Liu, J., Ketova, T., Fleming, J. T., Grover, V. K., Cooper, M. K., Litingtung, Y. and Chiang, C. (2010). Transventricular delivery of sonic hedgehog is essential to cerebellar ventricular zone development. *Proc. Natl. Acad. Sci. USA* **107**, 8422-8427.
Hunter, N. L. and Dymecki, S. M. (2007). Molecularly and temporally separable lineages form the hindbrain roof plate and contribute differentially to the choroid plexus. *Development* **134**, 3449-3460.
Imayoshi, I., Shimogori, T., Ohtsuka, T. and Kageyama, R. (2008). Hes genes and neurogenin regulate non-neural versus neural fate specification in the dorsal telencephalic midline. *Development* **135**, 2531-2541.
Johansson, P. A., Dziegielewska, K. M., Ek, C. J., Habgood, M. D., Møllgård, K., Potter, A., Schuliga, M. and Saunders, N. R. (2005). Aquaporin-1 in the choroid plexuses of developing mammalian brain. *Cell Tissue Res.* **322**, 353-364.
Johansson, P. A., Dziegielewska, K. M., Ek, C. J., Habgood, M. D., Liddelow, S. A., Potter, A. M., Stolp, H. B. and Saunders, N. R. (2006). Blood-CSF barrier function in the rat embryo. *Eur. J. Neurosci.* **24**, 65-76.
Johansson, P. A., Cappello, S. and Götz, M. (2010). Stem cells niches during development – lessons from the cerebral cortex. *Curr. Opin. Neurobiol.* **20**, 400-407.
Krubitzer, L. (2007). The magnificent compromise: cortical field evolution in mammals. *Neuron* **56**, 201-208.
Landsberg, R. L., Awatramani, R. B., Hunter, N. L., Farago, A. F., DiPietrantonio, H. J., Rodriguez, C. I. and Dymecki, S. M. (2005). Hindbrain rhombic lip is comprised of discrete progenitor cell populations allocated by Pax6. *Neuron* **48**, 933-947.
Lee, K. J., Dietrich, P. and Jessell, T. M. (2000). Genetic ablation reveals that the roof plate is essential for dorsal interneuron specification. *Nature* **403**, 734-740.
Lehtinen, M. K., Zappaterra, M. W., Chen, X., Yang, Y. J., Hill, A. D., Lun, M., Maynard, T., Gonzalez, D., Kim, S., Ye, P. et al. (2011). The cerebrospinal fluid provides a proliferative niche for neural progenitor cells. *Neuron* **69**, 893-905.
Liddelow, S. A., Dziegielewska, K. M., Ek, C. J., Johansson, P. A., Potter, A. M. and Saunders, N. R. (2009). Cellular transfer of macromolecules across the developing choroid plexus of Monodelphis domestica. *Eur. J. Neurosci.* **29**, 253-266.
Marques, F., Sousa, J. C., Coppola, G., Gao, F., Puga, R., Brentani, H., Geschwind, D. H., Sousa, N., Correia-Neves, M. and Palha, J. A. (2011). Transcriptome signature of the adult mouse choroid plexus. *Fluids Barriers CNS* **8**, 10.
Møllgård, K., Milinowska, D. H. and Saunders, N. R. (1976). Lack of correlation between tight junction morphology and permeability properties in developing choroid plexus. *Nature* **264**, 293-294.
Molnár, Z., Métin, C., Stoykova, A., Tarabykin, V., Price, D. J., Francis, F., Meyer, G., Dehay, C. and Kennedy, H. (2006). Comparative aspects of cerebral cortical development. *Eur. J. Neurosci.* **23**, 921-934.
Moon, S. M., Kim, S. A., Yoon, J. H. and Ahn, S. G. (2012). HOXC6 is deregulated in human head and neck squamous cell carcinoma and modulates Bcl-2 expression. *J. Biol. Chem.* **287**, 35678-35688.
Nakamura, T., Colbert, M. C. and Robbins, J. (2006). Neural crest cells retain multipotential characteristics in the developing valves and label the cardiac conduction system. *Circ. Res.* **98**, 1547-1554.
Nielsen, C. M. and Dymecki, S. M. (2010). Sonic hedgehog is required for vascular outgrowth in the hindbrain choroid plexus. *Dev. Biol.* **340**, 430-437.
Ninkovic, J., Pinto, L., Petricca, S., Lepier, A., Sun, J., Rieger, M. A., Schroeder, T., Cvekl, A., Favor, J. and Götz, M. (2010). The transcription factor Pax6 regulates survival of dopaminergic olfactory bulb neurons via crystallin αA. *Neuron* **68**, 682-694.
Omodei, D., Acampora, D., Mancuso, P., Prakash, N., Di Giovannantonio, L. G., Wurst, W. and Simeone, A. (2008). Anterior-posterior graded response to Otx2 controls proliferation and differentiation of dopaminergic progenitors in the ventral mesencephalon. *Development* **135**, 3459-3470.
Parada, C., Escolà-Gil, J. C. and Bueno, D. (2008). Low-density lipoproteins from embryonic cerebrospinal fluid are required for neural differentiation. *J. Neurosci. Res.* **86**, 2674-2684.
Perea-Gomez, A., Rhinn, M. and Ang, S. L. (2001). Role of the anterior visceral endoderm in restricting posterior signals in the mouse embryo. *Int. J. Dev. Biol.* **45**, 311-320.
Pinto, L., Drechsel, D., Schmid, M. T., Ninkovic, J., Irmler, M., Brill, M. S., Restani, L., Gianfranceschi, L., Cerri, C., Weber, S. N. et al. (2009). AP2gamma regulates basal progenitor fate in a region- and layer-specific manner in the developing cortex. *Nat. Neurosci.* **12**, 1229-1237.
Pöschl, J., Grammel, D., Dorostkar, M. M., Kretzschmar, H. A. and Schüller, U. (2012). Constitutive activation of β-Catenin in neural progenitors results in disrupted proliferation and migration of neurons within the central nervous system. *Dev. Biol.* (in press).
Prakash, N., Brodski, C., Naserke, T., Puelles, E., Gogoi, R., Hall, A., Panhuysen, M., Echevarria, D., Sussel, L., Weisenhorn, D. M. et al. (2006). A Wnt1-regulated genetic network controls the identity and fate of midbrain-dopaminergic progenitors in vivo. *Development* **133**, 89-98.

Puelles, E., Acampora, D., Lacroix, E., Signore, M., Annino, A., Tuorto, F., Filosa, S., Corte, G., Wurst, W., Ang, S. L. et al. (2003). Otx dose-dependent integrated control of antero-posterior and dorso-ventral patterning of midbrain. *Nat. Neurosci.* **6**, 453-460.

Puelles, E., Annino, A., Tuorto, F., Usiello, A., Acampora, D., Czerny, T., Brodski, C., Ang, S. L., Wurst, W. and Simeone, A. (2004). Otx2 regulates the extent, identity and fate of neuronal progenitor domains in the ventral midbrain. *Development* **131**, 2037-2048.

Rainer, J., Sanchez-Cabo, F., Stocker, G., Sturn, A. and Trajanoski, Z. (2006). CARMAweb: comprehensive R- and bioconductor-based web service for microarray data analysis. *Nucleic Acids Res.* **34**, W498-W503.

Sugiyama, S., Di Nardo, A. A., Aizawa, S., Matsuo, I., Volovitch, M., Prochiantz, A. and Hensch, T. K. (2008). Experience-dependent transfer of Otx2 homeoprotein into the visual cortex activates postnatal plasticity. *Cell* **134**, 508-520.

R Development Core Team (2005). *R: A Language and Environment for Statistical Computing*. Vienna: R Foundation for Statistical Computing.

von Frowein, J., Wizenmann, A. and Götz, M. (2006). The transcription factors Emx1 and Emx2 suppress choroid plexus development and promote neuroepithelial cell fate. *Dev. Biol.* **296**, 239-252.

Wilting, J. and Christ, B. (1989). An experimental and ultrastructural study on the development of the avian choroid plexus. *Cell Tissue Res.* **255**, 487-494.

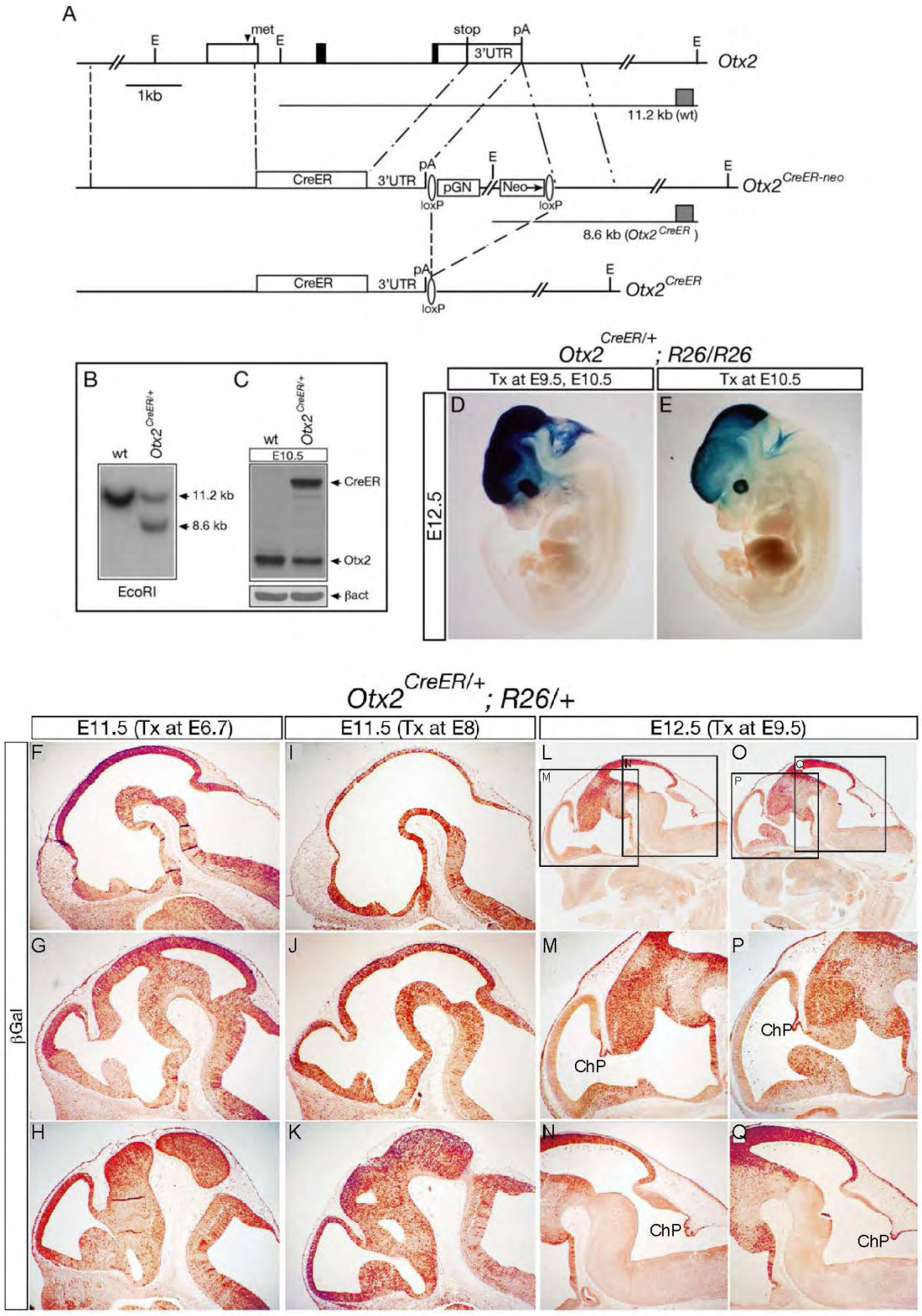

Fig. S1. The *Otx2CreER/+* mouse model. (**A**) For the *Otx2CreER/+* mouse model, the targeting molecule was obtained by replacing the genomic region spanning the entire *Otx2* coding sequence with the tamoxifen-inducible CreERT2 recombinase followed by the *Otx2* 3′UTR and polyadenylation signal (Feil et al., 1997). (**B**) Correct homologous recombination events in E14tg4a2 ES cells were ascertained by PCR and confirmed by Southern blot. The *neo* cassette was removed by crossing founder heterozygotes with a CMV-Cre mouse deleter strain. *Otx2CreER* mutant mice were bred in the B6D2 genetic background and genotyped with the following primers (5′-3′): wild-type allele, forward CTCCTTTAAAAGCCTGTGCCCAGCG and reverse CTGCGTAAGGCGGTTGCTTTAG; mutant allele, forward as for the wild-type allele, reverse CGATCCCTGAACATGTCCATCAGG. (**C-E**) The CreER protein level was similar to that of Otx2 as deduced by western blot of E10.5 *Otx2CreER/+* embryonic head extracts (C); and the activity was apparently quite efficient as revealed by X-Gal staining of *Otx2CreER/+;R26/+* embryos administered with Tamoxifen (Tx) at E9.5 (D) or/and sacrificed at E12.5 (D,E). (**F-Q**) Sagittal sections of X-Gal staining of *Otx2CreER/+;R26/+* embryos administered with Tx at E6.7 (F-H) or E8 (I-K) and sacrificed at E11.5, or with Tx administration at E9.5 and sacrificed at E12.5 (L-Q). ChP, choroid plexus.

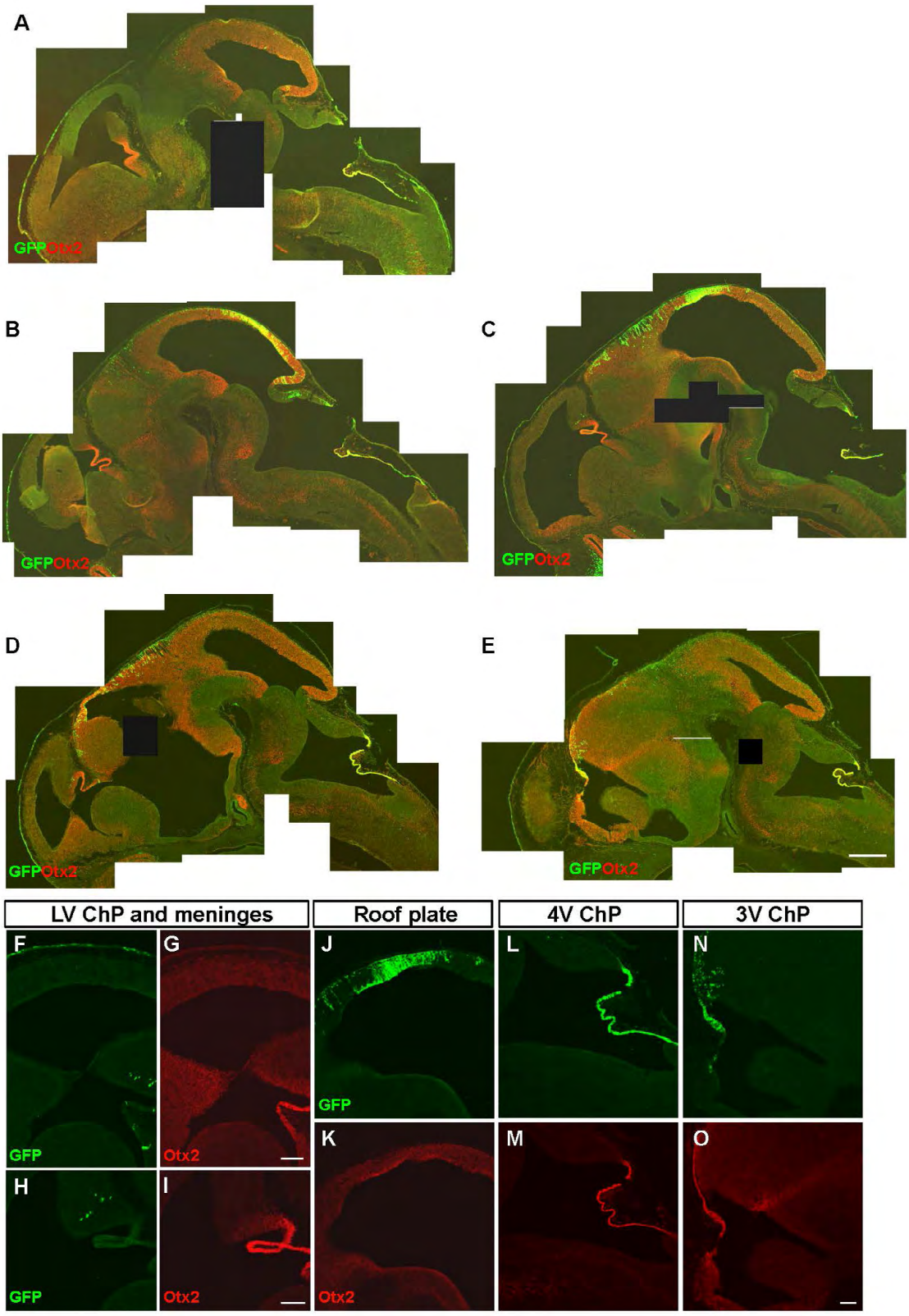

Fig. S2. Otx2 expression and Gdf7-Cre recombination pattern. (**A-E**) Composite images of sagittal sections from E12 Gdf7-Cre/CAG-GFP reporter embryos showing the distribution of GFP and Otx2. Scale bar: 200 µm. (**F-O**) Confocal images showing higher magnification of areas with high Otx2 expression and/or GFP reporter activity. Scale bars: 50 µm. LV ChP, lateral ventricular ChP; 3V and 4V, third and fourth ventricular ChP, respectively.

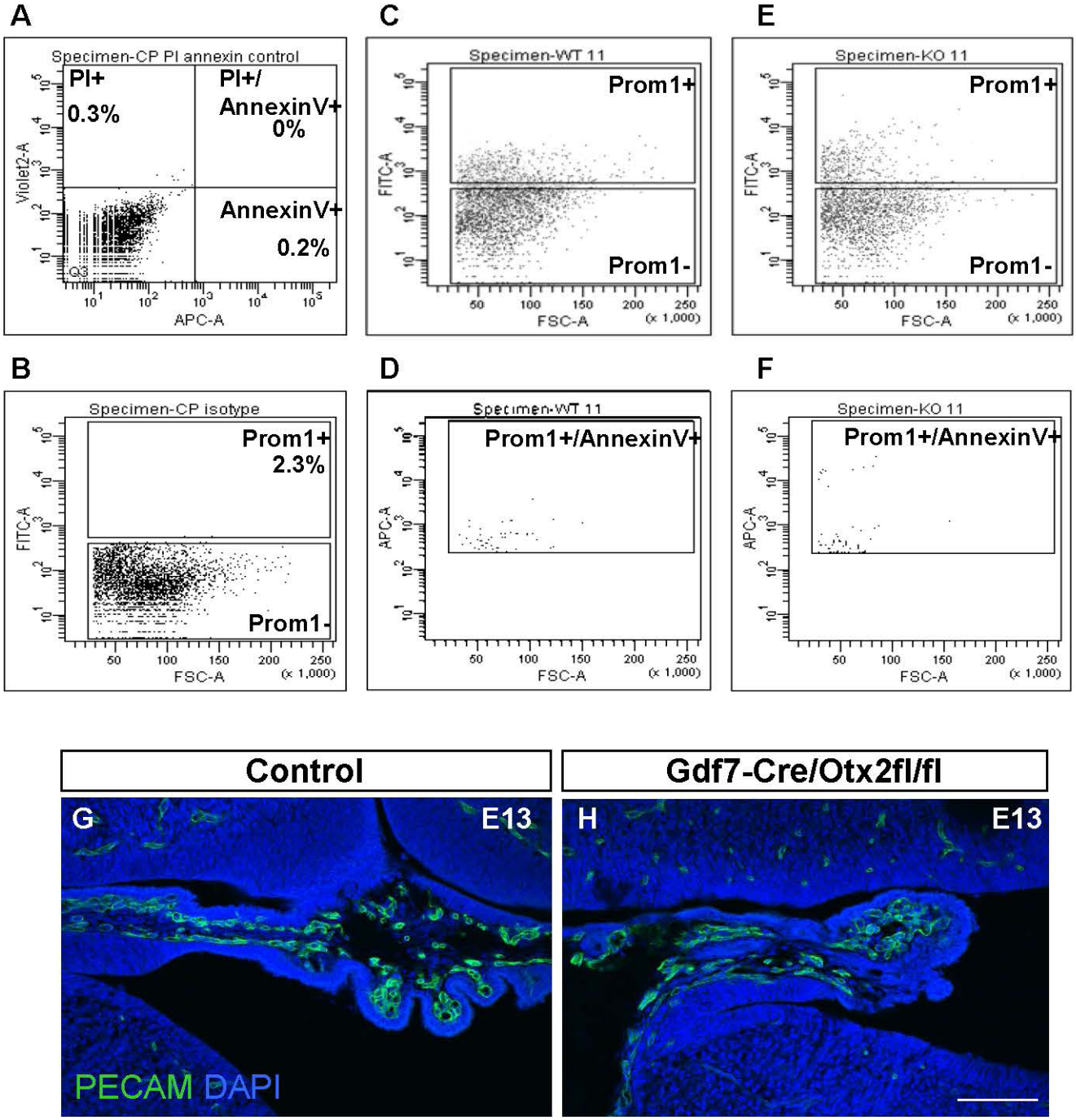

Fig. S3. Phenotype of the hindbrain choroid plexus in *Gdf7-Cre/Otx2*$^{fl/fl}$ mice. (**A**) Plot depicting unstained cells detected by the APC-A and Violet 2A lasers. This allowed for selection of the positive gates for annexin V and propidium iodide (PI), as depicted. The percentage of non-fluorescent cells included in the positive gates is shown for each population. (**B**) Plot depicting cells stained by the FITC-conjugated isotype control and detected by the FITC-A laser. The positive gate for prominin 1 was set as depicted. (**C-F**) Example plots from control (C,D) and *Gdf7-Cre/Otx2*$^{fl/fl}$ (E,F) choroid plexus depicting the prominin 1^+ cells (C,E) and the prominin 1^+ cells that were also positive for annexin V (D,F). (**G**,**H**) Micrographs depict coronal sections of hindbrain choroid plexus from control (G) and *Gdf7-Cre/Otx2*$^{fl/fl}$ (H) E13 embryos. Blood vessels were visualized by Pecam immunohistochemistry, nuclei were labeled with DAPI and analyzed using confocal imaging (*z*-stack). Scale bar: 100 µm.

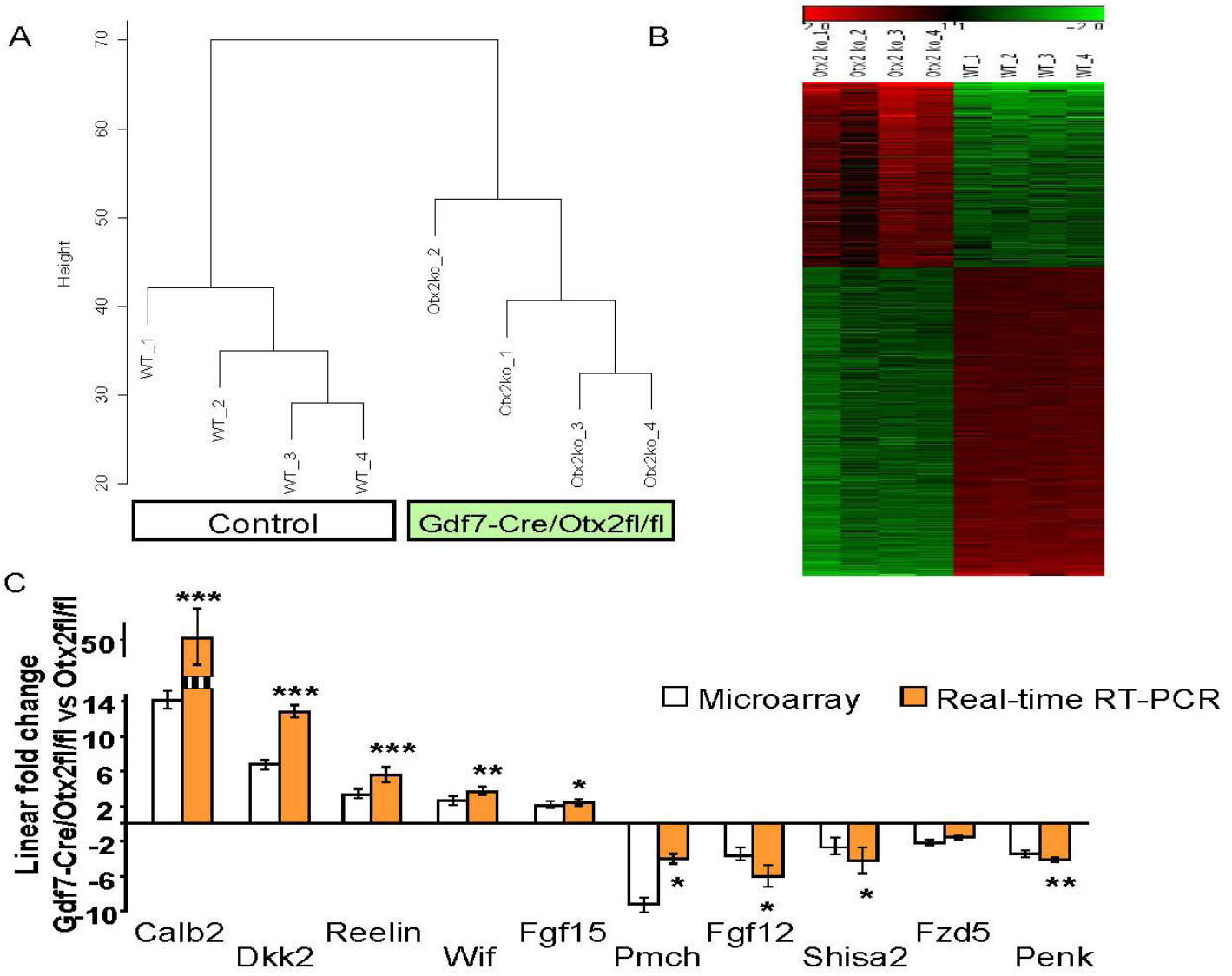

Fig. S4. Microarray analysis of hindbrain choroid plexus from E13 control and *Gdf7-Cre/Otx2*$^{fl/fl}$ mice. (**A**) Hierarchical cluster analysis of control (WT) and *Gdf7-Cre/Otx2*$^{fl/fl}$ (Ko) microarray data. (**B**) Heat map representing log2 expression data of significantly regulated probe sets. (**C**) Quantitative comparison of microarray results (white bars) with results from real-time RT-PCR (orange bars). n=4; *P<0.05, *P<0.01, *P<0.001; error bars indicate s.e.m.

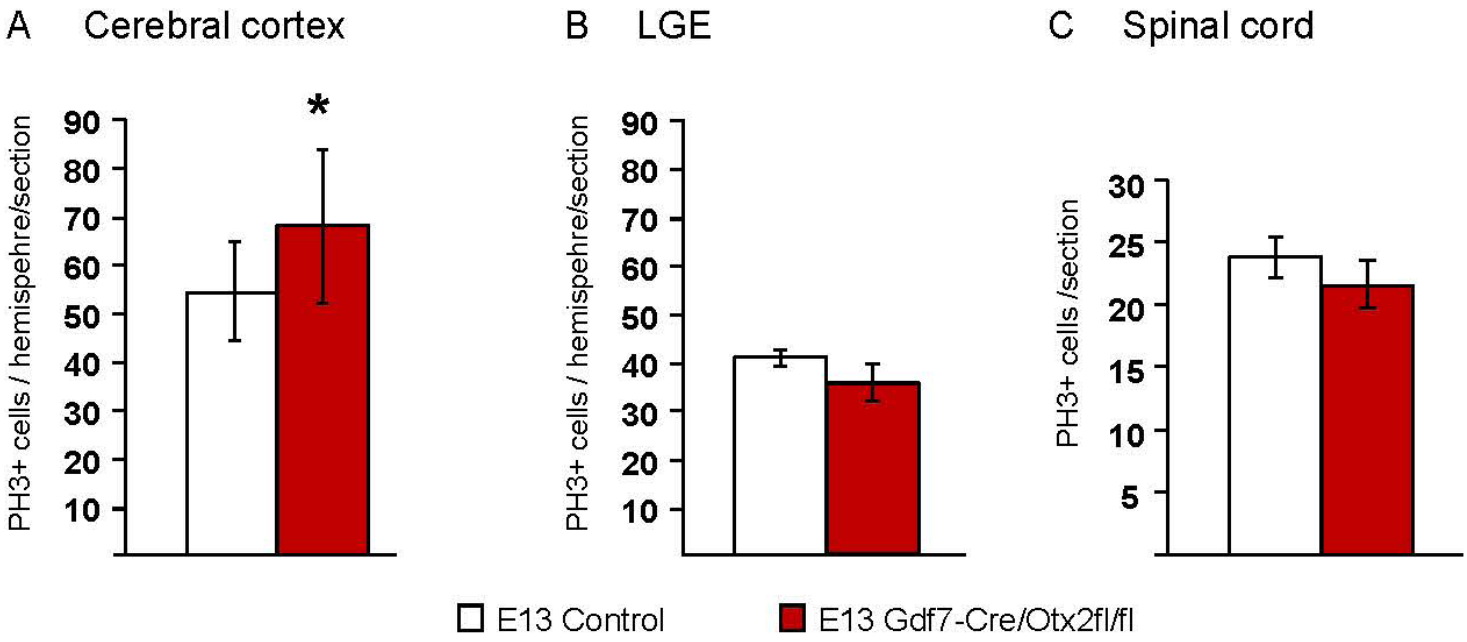

Fig. S5. Number of PH3$^+$ cells in apical progenitors in contact with the CSF. (**A-C**) PH3$^+$ cells were counted per hemisphere (for cortex, A, *n*=6 and LGE, B, *n*=4), and per section (spinal cord, C, *n*=4). A minimum of three sections per animal were counted. **P*<0.05.

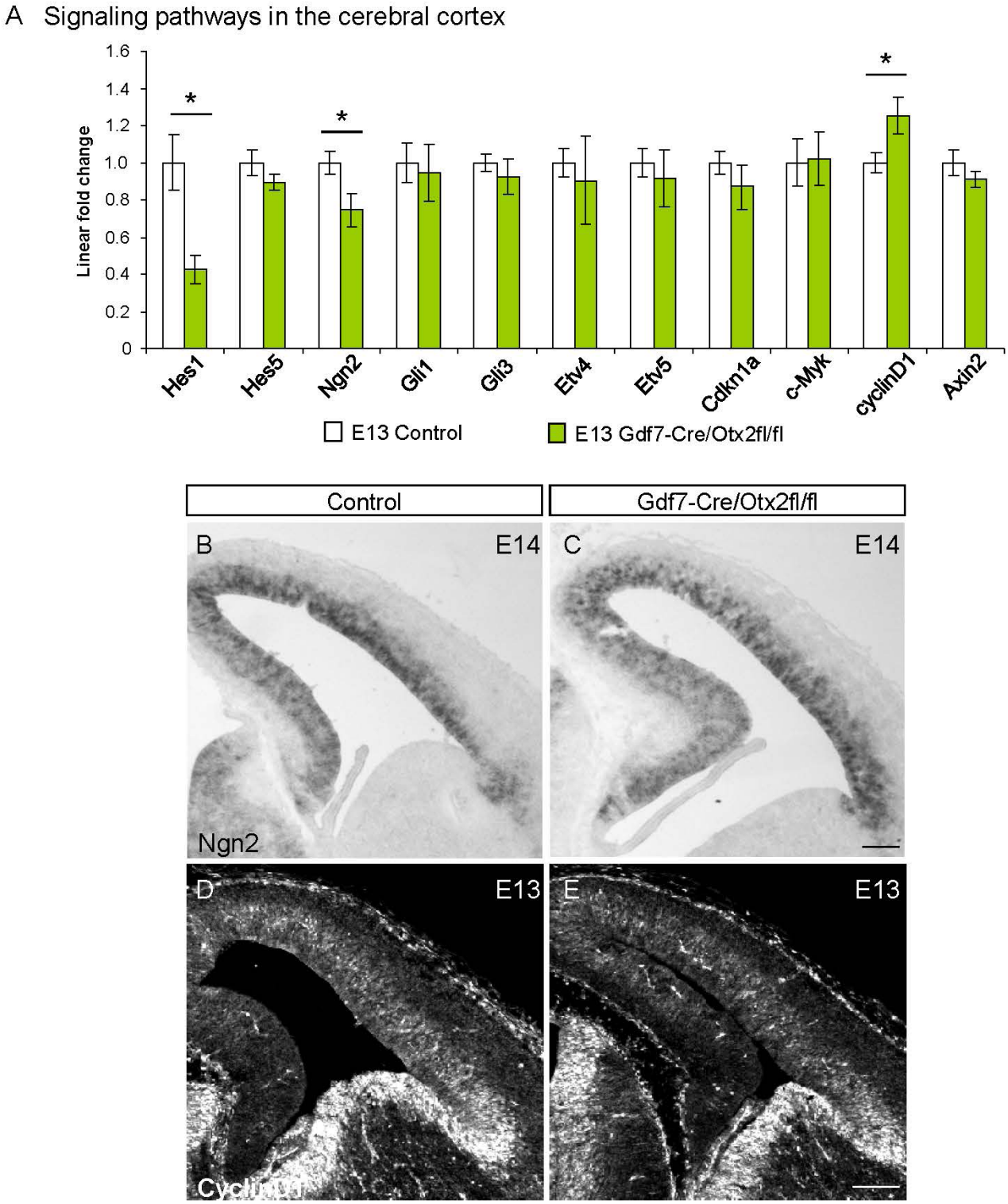

Fig. S6. Pathway activation in cortices of control and *Gdf7-Cre/Otx2*$^{fl/fl}$ mice. (**A**) Analysis of pathway activation, as measured by real-time RT-PCR, in cerebral cortex from control and *Gdf7-Cre/Otx2*$^{fl/fl}$ embryos. *n*=5. (**B-E**). Micrographs depict *Ngn2* in situ hybridization (B,C) and cyclin D1 immunohistochemistry (D,E) of coronal sections of cerebral cortex from control and *Gdf7-Cre/Otx2*$^{fl/fl}$ embryos. Scale bars: 100 µm.

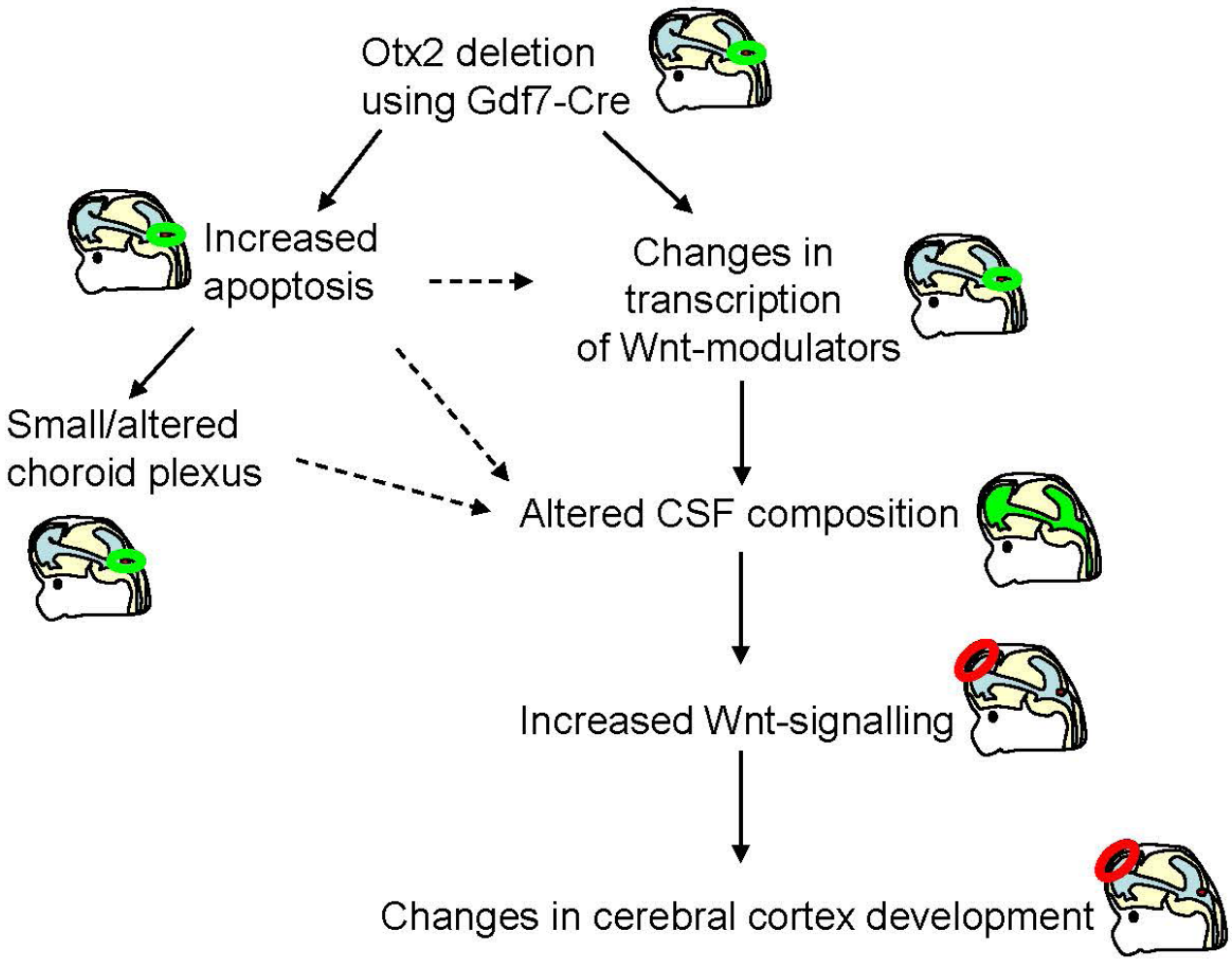

Fig. S7. Summary of the phenotypes of Gdf7-Cre mutants. Solid arrows indicate experimentally supported hypotheses and dashed arrows indicate other possible mechanisms. The phenotype observed in *Gdf7-Cre/Otx2*$^{fl/fl}$, where the altered hindbrain choroid plexus can affect the cerebral cortex, occurs during a very particular time in development when the ventricular system is still enclosed and has no major bulk flow of fluid passing through it. This allows molecules secreted into the CSF to more easily access cells along the entire ventricular system.

Table S1. Differentially* upregulated genes in *Gdf7-Cre/Otx2*$^{fl/fl}$ choroid plexus

Probe set	Gene symbol	Entrez	Linear ratio	Average expression *Otx2* ko	Average expression WT
1451129_at	Calb2	12308	14.12	1567	111
1435239_at	Gria1	14799	10.22	262	26
1455498_at	Gpr50	14765	10.22	74	7
1449158_at	Kcnk2	16526	3.95	822	208
1448397_at	Gjb6	14623	3.67	1420	387
1429175_at	Tmem178	68027	3.41	517	152
1423271_at	Gjb2	14619	3.34	1429	427
1448261_at	Cdh1	12550	3.23	298	92
1433532_a_at	Mbp	17196	3.22	152	47
1453128_at	Lyve1	114332	2.99	292	98
1416003_at	Cldn11	18417	2.94	1100	374
1455000_at	Gpr68	238377	2.63	115	44
1451424_at	Gabrp	216643	2.57	138	54
1448213_at	Anxa1	16952	2.57	518	202
1445534_at	Flnb	286940	2.42	111	46
1427465_at	Atp1a2	98660	2.32	649	280
1415832_at	Agtr2	11609	2.28	112	49
1424308_at	Slc24a3	94249	2.27	317	140
1429076_a_at	Gdpd2	71584	2.19	257	117
1455462_at	Adcy2	210044	2.18	377	173
1459713_s_at	Ano1	101772	2.13	336	158
1418240_at	Gbp2	14469	2.13	125	59
1426301_at	Alcam	11658	2.10	1345	640
1415800_at	Gja1	14609	2.10	2979	1422
1460694_s_at	Svil	225115	2.09	1773	847
1426452_a_at	Rab30	75985	2.09	169	81
1434728_at	Gria3	53623	2.08	167	80
1458015_at	Megf11	214058	2.07	259	125
1443119_at	Grm7	108073	2.07	120	58
1416855_at	Gas1	14451	2.05	3670	1786
1417143_at	Lpar1	14745	2.05	291	141
1434447_at	Met	17295	2.05	96	47
1435888_at	Egfr	13649	2.02	374	185
1460431_at	Gcnt1	14537	7.13	496	70
1434779_at	Cbln2	12405	3.79	385	102
1450112_a_at	Gas2	14453	3.07	442	144
1440879_at	Abca9	217262	3.05	991	325
1436734_at	E130309F12Rik	272031	3.02	61	20
1448265_x_at	Mpzl2	14012	2.97	78	26
1452227_at	2310045A20Rik	231238	2.55	503	197
1457423_at	LOC675405	338370	2.51	189	75
1438975_x_at	Zdhhc14	224454	2.28	231	101

1428875_at	Golim4	73124	2.12	1812	857
1451547_at	Iyd	70337	2.10	142	68
1434776_at	Sema5a	20356	2.09	77	37
1429693_at	Dab2	13132	2.07	173	84
1432360_a_at	Tmtc4	70551	2.06	256	124
1428089_at	Slitrk1	76965	2.04	186	91
1419693_at	Colec12	140792	2.02	816	403
1425039_at	Itgbl1	223272	3.09	67	22
1425575_at	Epha3	13837	2.16	316	146
1460258_at	Lect1	16840	6.35	357	56
1429459_at	Sema3d	108151	2.61	113	43
1447845_s_at	Vnn1	22361	2.39	73	31
1449465_at	Reln	19699	3.19	1878	588
1430352_at	Adamts9	101401	2.11	60	28
1449254_at	Spp1	20750	2.99	641	214
1449319_at	Rspo1	192199	2.99	481	161
1450728_at	Fjx1	14221	2.90	647	223
1448823_at	Cxcl12	20315	2.16	973	451
1416625_at	Serping1	12258	2.10	644	306
1423250_a_at	Tgfb2	21808	2.05	419	204
1417497_at	Cp	12870	2.02	96	47
1437218_at	Fn1	14268	2.49	114	46
1448598_at	Mmp17	23948	2.19	194	89
1433428_x_at	Tgm2	21817	2.03	480	236
1449979_a_at	Spock3	72902	4.80	110	23
1460412_at	Fbln7	70370	4.25	199	47
1438966_x_at	Fmod	14264	3.62	179	49
1449368_at	Dcn	13179	2.49	2743	1100
1415935_at	Smoc2	64074	2.33	204	87
1452968_at	Cthrc1	68588	2.30	1528	665
1448228_at	Lox	16948	2.26	406	180
1439827_at	Adamts12	239337	2.18	995	456
1420484_a_at	Vtn	22370	2.17	791	364
1438020_at	Hapln1	12950	2.16	95	44
1423407_a_at	Fbln2	14115	2.15	936	435
1417455_at	Tgfb3	21809	2.11	745	352
1450782_at	Wnt4	22417	2.07	737	356
1422831_at	Fbn2	14119	2.03	1348	665
1420512_at	Dkk2	56811	6.87	2214	322
1422606_at	C1qtnf3	81799	5.63	444	79
1419383_at	S100b	20203	4.41	146	33
1416371_at	Apod	11815	3.01	1016	338
1433529_at	Pamr1	210622	2.88	189	66
1425425_a_at	Wif1	24117	2.64	312	118
1419717_at	Sema3e	20349	2.60	366	141
1430700_a_at	Pla2g7	27226	2.27	884	390
1456335_at	Gm106	226866	2.24	145	65

1447839_x_at	Adm	11535	2.15	88	41
1433653_at	Fam20a	208659	2.13	102	48
1450085_at	Angptl2	26360	2.10	376	179
1418376_at	Fgf15	14170	2.06	523	254
1448201_at	Sfrp2	20319	2.05	1420	692
1448428_at	Nbl1	17965	2.05	496	242
1436755_at	Itih5	209378	2.04	109	54
1448929_at	F13a1	74145	2.03	1725	848
1448972_at	Gria1	100044431	7.79	119	15
1455147_at			6.86	468	68
1434342_at	S100b	20203	5.23	127	24
1457140_s_at	Rassf10	78748	5.22	84	16
1453192_at	Fam101a	73121	4.90	219	45
1456084_x_at	Fmod	14264	4.82	2409	500
1455393_at	Cp	12870	4.61	502	109
1448734_at	Cp	12870	4.50	454	101
1415939_at	Fmod	14264	4.34	825	190
1417495_x_at	Cp	12870	4.18	781	187
1437685_x_at	Fmod	14264	4.17	778	187
1437324_x_at	Fmod	14264	4.17	680	163
1417494_a_at	Cp	12870	4.08	1008	247
1437718_x_at	Fmod	14264	4.04	762	189
1417504_at	Calb1	12307	3.90	80	21
1436733_at	E130309F12Rik	272031	3.75	226	60
1429918_at	Arhgap20	244867	3.65	533	146
1416236_a_at	Mpzl2	14012	3.55	55	15
1429379_at	Lyve1	114332	3.51	1086	309
1419665_a_at	Nupr1	56312	3.44	281	82
1418486_at	Vnn1	22361	3.42	211	62
1416561_at	Gad1	14415	3.42	144	42
1449350_at	Osr1	23967	3.34	1091	327
1417496_at	Cp	12870	3.23	136	42
1427522_at	Arhgap20	244867	3.07	667	217
1422733_at	Fjx1	14221	3.05	308	101
1444432_at	D330040H18Rik	320847	2.98	60	20
1455136_at	Atp1a2	98660	2.93	393	134
1441693_at	Adamts3	330119	2.90	479	165
1443823_s_at	Atp1a2	98660	2.84	776	273
1457042_at	AI256396	58871	2.82	1214	431
1438042_at	Shox2	20429	2.77	122	44
1452308_a_at	Atp1a2	98660	2.76	356	129
1435399_at	Synpo2	118449	2.75	218	79
1448735_at	Cp	12870	2.73	263	96
1443921_at	Ranbp3l	223332	2.72	1065	392
1417788_at	Sncg	20618	2.66	219	82
1442226_at	Sema3e	20349	2.63	251	95
1441881_x_at	Fam101a	73121	2.62	334	128

1455707_at	Ranbp3l	223332	2.60	262	101
1419118_at	LOC100045106	100045106	2.58	226	88
1434893_at	Atp1a2	98660	2.52	288	114
1416077_at	Adm	11535	2.52	90	36
1438861_at	Bnc2	242509	2.51	582	232
1416121_at	Lox	16948	2.49	927	372
1422789_at	Aldh1a2	19378	2.47	289	117
1416762_at	S100a10	20194	2.43	1627	671
1437466_at	Alcam	11658	2.41	1121	465
1438619_x_at	Zdhhc14	224454	2.40	300	125
1437422_at	Sema5a	20356	2.39	150	63
1437614_x_at	Zdhhc14	224454	2.39	232	97
1439774_at	Prrx1	18933	2.36	187	79
1460330_at	Anxa3	11745	2.36	1158	490
1434025_at			2.36	320	136
1445758_at			2.34	683	292
1437467_at	Alcam	11658	2.33	724	311
1455090_at	Angptl2	26360	2.32	3143	1357
1429987_at	9930013L23Rik	80982	2.32	104	45
1453201_at	Rassf10	78748	2.31	110	48
1444564_at	Apod	100047583	2.31	91	39
1423505_at	Tagln	21345	2.30	419	182
1439852_at			2.30	235	102
1419666_x_at	Nupr1	56312	2.29	122	53
1435906_x_at	Gbp2	14469	2.28	179	79
1436713_s_at	Meg3	17263	2.25	426	190
1425526_a_at	Prrx1	18933	2.22	382	172
1426300_at	Alcam	11658	2.20	1175	534
1452183_a_at	Meg3	17263	2.20	2009	915
1429567_at	Rassf10	78748	2.19	87	40
1422573_at	Ampd3	11717	2.18	87	40
1452905_at	Meg3	17263	2.18	2109	967
1456642_x_at	S100a10	20194	2.18	1191	547
1418135_at	Aff1	17355	2.17	243	112
1442800_x_at	Fam181b	58238	2.17	151	70
1453084_s_at	Col22a1	69700	2.16	600	278
1424932_at	Egfr	13649	2.16	135	62
1435603_at	Sned1	208777	2.15	1112	517
1455900_x_at	Tgm2	21817	2.15	360	167
1426758_s_at	Meg3	17263	2.14	1238	578
1438676_at	Mpa2l	100702	2.13	105	49
1425528_at	Prrx1	18933	2.13	525	247
1437277_x_at	Tgm2	21817	2.10	592	283
1423319_at	Hhex	15242	2.09	347	166
1438303_at	Tgfb2	21808	2.09	137	66
1428113_at	Tmtc4	70551	2.08	2143	1030
1428662_a_at	Hopx	74318	2.07	2297	1108

1416454_s_at	Acta2	11475	2.07	643	310
1436766_at	Luc7l2	192196	2.06	339	165
1444198_at			2.06	250	121
1448494_at	Gas1	14451	2.06	1093	531
1444302_at	Glt8d4	100048436	2.05	188	92
1452382_at	Dnm3os	474332	2.05	63	31
1425995_s_at	Wt1	22431	2.05	118	58
1451287_s_at	Aif1l	108897	2.04	246	121
1448891_at	Fcrls	80891	2.02	483	239

*Ratio >2-fold, average expression in at least one group >50, FDR<10%.

Table S2. Differentially* downregulated genes in *Gdf7-Cre/Otx2*$^{fl/fl}$ choroid plexus

Probe set	Gene symbol	Entrez	Linear ratio	Average expression *Otx2* ko	Average expression WT
1429361_at	Pmch	110312	0.11	115	1011
1460601_at	Myrip	245049	0.19	77	395
1452298_a_at	Myo5b	17919	0.21	79	369
1425038_at	Slc22a9	207151	0.23	98	433
1455627_at	Col8a1	12837	0.23	426	1827
1418190_at	Pon1	18979	0.23	30	126
1418440_at	Col8a1	12837	0.24	197	812
1415856_at	Emb	13723	0.24	186	759
1424938_at	Steap1	70358	0.25	23	91
1436076_at	Dlgap1	224997	0.25	47	185
1456555_at	Ccdc67	234964	0.26	275	1075
1450830_a_at	Pde6c	110855	0.26	110	423
1455114_at	Ccno	218630	0.27	124	468
1434719_at	A2m	232345	0.27	571	2117
1440270_at	Fgf12	14167	0.27	48	175
1435392_at	Wdr17	244484	0.27	33	120
1415857_at	Emb	13723	0.27	162	592
1423627_at	Nqo1	18104	0.27	102	373
1439899_at	Galnt13	271786	0.29	67	234
1455374_at	Kcnj3	16519	0.29	20	71
1427038_at	Penk	18619	0.30	1567	5311
1445679_at			0.30	953	3228
1420763_at	Klk4	56640	0.30	143	473
1457045_at	Galnt13	271786	0.30	48	159
1448786_at	LOC100045163	100045163	0.31	186	601
1421093_at	Slc7a10	53896	0.31	204	658
1429348_at	Sema3c	20348	0.31	753	2428
1416688_at	Snap91	20616	0.31	319	1024
1444946_at			0.31	267	853
1436432_at	B230343J05Rik	320320	0.31	19	60
1417946_at	Abhd3	106861	0.32	150	473
1419261_at	Acad8	66948	0.32	204	643
1436274_at	Mrap2	244958	0.32	45	139
1440354_at	Elovl7	74559	0.32	30	93
1455083_at	Atp11c	320940	0.32	383	1192
1434685_at	D3Bwg0562e	229791	0.33	127	391
1417672_at	Slc4a10	94229	0.33	1465	4504
1443959_at	Tmem72	319776	0.33	106	326
1450477_at	Htr2c	15560	0.33	48	147
1427247_at	D3Bwg0562e	229791	0.33	779	2365
1457696_at	Rilp	280408	0.33	174	525
1424098_at	Elovl7	74559	0.33	97	295
1436332_at	Hspb6	243912	0.33	276	833

1450389_s_at	Pip5k1b	18719	0.33	80	240
1437029_at	Tacr3	21338	0.33	84	253
1447819_x_at	Col8a1	12837	0.33	453	1363
1434295_at	Rasgrp1	19419	0.33	47	142
1421834_at	Pip5k1b	18719	0.34	242	722
1421014_a_at	Clybl	69634	0.34	575	1714
1454104_a_at	Slc16a9	66859	0.34	26	78
1434760_at	Lrrtm3	216028	0.34	26	77
1437698_at	Myo5b	17919	0.34	40	119
1418310_a_at	Rlbp1	19771	0.34	66	196
1441891_x_at	Elovl7	74559	0.34	189	560
1435447_at	Mip	17339	0.34	51	149
1422734_a_at	Myb	17863	0.34	24	70
1455379_at	Dnali1	75563	0.34	221	647
1450194_a_at	Myb	17863	0.34	97	284
1421429_a_at	Npnt	114249	0.34	124	363
1451693_a_at	Fgf12	14167	0.34	87	254
1420405_at	Slco1a4	28250	0.34	285	830
1427775_at	Defb10	246085	0.35	175	506
1429726_at	Slc16a9	66859	0.35	251	720
1434766_at	Prkaa2	108079	0.35	162	465
1441091_at	Elovl7	74559	0.35	34	96
1434592_at	Slc16a10	72472	0.35	548	1558
1429135_at	1110059M19Rik	68800	0.35	635	1797
1452277_at	Arsg	74008	0.35	265	748
1436127_at	Crhbp	12919	0.35	45	127
1429727_at	Slc16a9	66859	0.36	297	837
1424097_at	Elovl7	74559	0.36	171	475
1417329_at	Slc23a2	54338	0.36	664	1851
1420919_at	Sgk3	170755	0.36	438	1213
1426561_a_at	Npnt	114249	0.36	233	640
1423258_at	Syt9	60510	0.36	294	807
1450725_s_at	Car14	23831	0.36	387	1061
1419262_at	Acad8	66948	0.37	300	818
1426560_a_at	Npnt	114249	0.37	321	868
1428663_at	Sgms2	74442	0.37	484	1310
1460250_at	Sostdc1	66042	0.37	1127	3047
1429105_at	Dlgap1	224997	0.37	45	120
1417900_a_at	Vldlr	22359	0.37	174	466
1420402_at	Atp2b2	11941	0.37	78	208
1433888_at	Atp2b2	11941	0.37	176	469
1442733_at	4922501C03Rik	382090	0.38	71	190
1456883_at	Stox1	216021	0.38	57	150
1421317_x_at	Myb	17863	0.38	165	435
1440312_at	Elovl7	74559	0.38	66	174
1431253_s_at	Tbc1d9	71310	0.38	124	325
1445328_at	Col4a4	12829	0.38	75	197

1423852_at	Shisa2	219134	0.38	78	204
1423851_a_at	Shisa2	219134	0.38	34	89
1442645_at	Atp2b3	320707	0.39	62	161
1451532_s_at	Steap1	70358	0.39	128	333
1416361_a_at	Dync1i1	13426	0.39	174	451
1419139_at	Gdf5	14563	0.39	206	533
1437609_at	Ube2u	381534	0.39	56	144
1440250_at	Col4a4	12829	0.39	47	121
1457314_at	L1td1	381591	0.39	38	97
1439855_at	Tmtc1	387314	0.39	68	175
1427002_s_at	Arsg	74008	0.39	492	1270
1434170_at	Decaf12l1	245404	0.39	601	1552
1426712_at	Slc6a15	103098	0.39	2214	5713
1425581_s_at	Galnt7	108150	0.39	112	288
1422750_a_at	Zmynd10	114602	0.39	235	602
1450702_at	Hfe	15216	0.39	172	439
1431450_at	4930444P10Rik	75799	0.39	39	100
1438097_at	Rab20	19332	0.39	54	137
1430351_at	Spata18	73472	0.39	37	94
1455267_at	Esrrg	26381	0.40	283	717
1438779_at	Col4a3	12828	0.40	64	162
1440803_x_at	Tacr3	21338	0.40	176	441
1422645_at	Hfe	15216	0.40	407	1023
1455214_at	Mitf	17342	0.40	555	1391
1435860_at	Slc5a6	330064	0.40	89	222
1453352_at	Atp10b	319767	0.40	127	318
1436368_at	Slc16a10	72472	0.40	986	2441
1433750_at	Slc31a1	20529	0.40	529	1309
1426442_at	Gpm6a	234267	0.40	254	628
1436611_at	Slc39a12	277468	0.41	166	408
1429831_at	Pik3ap1	83490	0.41	103	254
1436319_at	Sulf1	240725	0.41	985	2419
1443899_at	4922501C03Rik	382090	0.41	170	416
1424906_at	Pqlc3	217430	0.41	175	428
1418453_a_at	Atp1b1	11931	0.41	415	1016
1425518_at	Rapgef4	56508	0.41	69	168
1455422_x_at	Sept4	18952	0.41	160	389
1441389_at			0.41	44	108
1448729_a_at	Sept4	18952	0.41	188	456
1443933_at	Tc2n	74413	0.41	36	88
1443723_at	Trpm3	226025	0.41	622	1509
1451156_s_at	Vldlr	22359	0.41	45	110
1455501_at	Slc2a12	353169	0.41	80	192
1439026_at	Trpm3	226025	0.41	497	1199
1435911_s_at	Slc2a12	353169	0.41	529	1276
1451053_a_at	Mdm1	17245	0.42	150	360
1423523_at	Aass	30956	0.42	75	180

1449588_at	Abca4	11304	0.42	312	750
1420696_at	Sema3c	20348	0.42	43	103
1457766_at	Wfdc6a	209351	0.42	24	56
1426318_at	Serpinb1b	282663	0.42	771	1844
1424900_at	LOC100048058	100048058	0.42	373	892
1449179_at	Pdc	20028	0.42	36	87
1455923_at	Kctd8	243043	0.42	73	174
1426576_at	Sgms1	208449	0.42	259	615
1425900_at	Hkdc1	216019	0.42	139	330
1426959_at	Bdh1	71911	0.42	98	233
1452232_at	Galnt7	108150	0.42	559	1326
1439332_at	Ddit4l	73284	0.42	147	349
1437724_x_at	Pitpnm1	18739	0.42	1141	2697
1429074_at	1700026D08Rik	75556	0.42	104	246
1435893_at	Vldlr	22359	0.42	127	299
1439036_a_at	Atp1b1	11931	0.42	607	1430
1426044_a_at	Prkcq	18761	0.43	252	593
1451539_at	Baiap2l1	66898	0.43	125	294
1422438_at	Ephx1	13849	0.43	175	410
1426908_at	Galnt7	108150	0.43	410	961
1448873_at	Ocln	18260	0.43	657	1536
1457215_at	Gm13111	100042178	0.43	77	179
1429228_at	4930534B04Rik	75216	0.43	50	116
1428046_a_at	Zfx	22764	0.43	44	103
1425181_at	Sgip1	73094	0.43	41	96
1436350_at	Fam171b	241520	0.43	328	767
1438200_at	Sulf1	240725	0.43	1735	4047
1449340_at	Sostdc1	66042	0.43	1808	4209
1417801_a_at	Ppfibp2	19024	0.43	260	605
1429463_at	Prkaa2	108079	0.43	136	316
1459122_at	Spef2	320277	0.43	39	91
1460043_at			0.43	132	307
1445630_at			0.43	530	1233
1437967_at			0.43	198	459
1460036_at	Ap1s2	108012	0.43	461	1071
1455285_at	Slc31a1	20529	0.43	276	640
1454869_at	Decaf12l1	245404	0.43	156	361
1443960_at			0.43	54	124
1444139_at	Ddit4l	73284	0.43	129	297
1429464_at	Prkaa2	108079	0.43	50	115
1422025_at	Mitf	17342	0.43	67	155
1451499_at	Cadps2	320405	0.43	208	479
1430283_s_at	Lrrc67	69312	0.44	70	160
1434430_s_at	Adora2b	100045233	0.44	22	51
1429308_at	Prdm16	70673	0.44	237	544
1424280_at	Mospd1	70380	0.44	500	1145
1418441_at	Col8a1	12837	0.44	42	95

1452609_at	1190005I06Rik	68918	0.44	140	320
1444238_at			0.44	23	52
1456792_at	LOC100045317	100045317	0.44	99	225
1454965_at			0.44	600	1365
1442169_at	Vldlr	22359	0.44	77	175
1431302_a_at	Nudt7	67528	0.44	419	951
1457402_at			0.44	30	67
1434465_x_at	Vldlr	22359	0.44	361	820
1452804_at	Morn5	75495	0.44	262	594
1440870_at	Prdm16	70673	0.44	950	2151
1440220_at			0.44	368	834
1424977_at	Lrrc67	69312	0.44	59	135
1452355_at	Rd3	74023	0.44	156	351
1449203_at	Slco1a5	108096	0.44	45	102
1436237_at	Ttc9	69480	0.45	251	563
1438258_at	Vldlr	22359	0.45	182	408
1455618_x_at	Tspan33	232670	0.45	537	1203
1436499_at	Sgms1	208449	0.45	521	1167
1424951_at	Baiap2l1	66898	0.45	311	696
1455664_at	Rtn4rl1	237847	0.45	75	167
1449411_at	Dscam	13508	0.45	58	129
1425213_at	Fam81a	76886	0.45	580	1297
1430307_a_at	LOC677317	17436	0.45	181	404
1425760_a_at	Pitpnm1	18739	0.45	365	815
1452107_s_at	Npnt	114249	0.45	1606	3584
1460580_at	Pcnx	54604	0.45	289	643
1428811_at	Wfikkn2	278507	0.45	652	1448
1428680_at	Cds1	74596	0.45	284	631
1460734_at	Col9a3	12841	0.45	1363	3020
1436474_at	Clec18a	353287	0.45	52	114
1451527_at	Pcolce2	76477	0.45	213	472
1426575_at	Sgms1	208449	0.45	97	215
1446747_at	Spef2	320277	0.45	27	60
1428485_at	Car12	76459	0.46	920	2023
1453152_at	Mamdc2	71738	0.46	161	353
1451608_a_at	Tspan33	232670	0.46	399	875
1435396_at	Stxbp6	217517	0.46	137	300
1440472_at	Spag17	74362	0.46	30	65
1424698_s_at	Gca	227960	0.46	62	135
1436203_a_at	1110059G02Rik	68786	0.46	99	217
1453250_at	LOC100046859	70853	0.46	35	78
1460693_a_at	Col9a3	12841	0.46	637	1391
1449907_at	Bcmo1	63857	0.46	32	70
1434800_at	Sv2b	64176	0.46	84	182
1453027_at	Dlgap1	224997	0.46	49	107
1429861_at	Pcdh9	211712	0.46	314	680
1436633_at			0.46	57	123

1436656_at	BC062109	231503	0.46	68	147
1430896_s_at	Nudt7	67528	0.46	210	455
1450995_at	Folr1	14275	0.46	2261	4890
1443327_at	D130043K22Rik	210108	0.46	85	183
1421833_at	Pip5k1b	18719	0.46	170	366
1455061_a_at	Acaa2	52538	0.46	351	756
1435553_at	Pdzd2	68070	0.47	210	450
1417780_at	Lass4	67260	0.47	484	1040
1439194_at	C030048H21Rik	77481	0.47	89	191
1428960_at	Enkur	71233	0.47	503	1078
1433551_at	Vat1l	270097	0.47	1763	3775
1452106_at	Npnt	114249	0.47	3264	6988
1435275_at	Cox6b2	333182	0.47	834	1785
1419393_at	Abcg5	27409	0.47	642	1374
1451152_a_at	Atp1b1	11931	0.47	694	1485
1456741_s_at	Gpm6a	234267	0.47	772	1650
1450931_at	Dock9	105445	0.47	268	573
1429816_at	Armc3	70882	0.47	311	663
1435420_at	Slc4a5	232156	0.47	878	1870
1418674_at	Osmr	18414	0.47	301	640
1436552_at	Jakmip2	76217	0.47	216	458
1441966_at	Trpm3	226025	0.47	184	391
1428973_s_at	Tctex1d2	66061	0.47	703	1486
1436126_at	Dnali1	75563	0.47	117	248
1418808_at	Rdh5	19682	0.47	150	316
1429815_at	Armc3	70882	0.47	172	362
1418445_at	Slc16a2	20502	0.47	1003	2117
1429851_at	1700003M02Rik	69329	0.48	210	441
1416632_at	LOC677317	17436	0.48	328	689
1428599_at	Kndc1	76484	0.48	60	126
1437187_at	E2f7	52679	0.48	404	848
1448024_at	Npr3	18162	0.48	223	468
1436916_at	Tmem108	81907	0.48	379	795
1438428_at	Jph1	57339	0.48	80	168
1455162_at	Ttc39a	230603	0.48	78	162
1449563_at	Cntn1	12805	0.48	978	2040
1452325_at	Trp73	22062	0.48	127	265
1417782_at	Lass4	67260	0.48	87	181
1457352_x_at	Svopl	320590	0.48	91	189
1449167_at	Epb4.1l4a	13824	0.48	390	809
1418870_at	4930579J09Rik	67752	0.48	247	511
1428622_at	Depdc6	97998	0.48	74	153
1418446_at	Slc16a2	20502	0.48	714	1475
1418994_at	Gtsf1l	68236	0.48	84	172
1455377_at	Ttll7	70892	0.49	58	120
1420638_at	Prps2	110639	0.49	111	229
1432217_a_at	Wdr16	71860	0.49	87	179

1456515_s_at	Tcfl5	277353	0.49	65	133
1453119_at	Otud1	71198	0.49	108	221
1421844_at	Il1rap	16180	0.49	104	213
1436481_at			0.49	67	137
1428866_at	2810037O22Rik	72711	0.49	407	836
1452365_at	Csgalnact1	234356	0.49	111	227
1418958_at	Amac1	56293	0.49	223	457
1437094_x_at	Dnaic1	68922	0.49	213	437
1418589_a_at	Mlf1	17349	0.49	1038	2127
1453868_at	Ccdc11	74453	0.49	241	494
1459274_at	Gpr135	238252	0.49	28	56
1460107_at	Fam154b	330577	0.49	117	240
1438974_x_at	Pitpnm1	18739	0.49	32	65
1455872_at	Fam167a	219148	0.49	126	257
1420403_at	Atp2b2	11941	0.49	84	171
1442823_at	Shank2	210274	0.49	119	243
1450484_a_at	Cmpk2	22169	0.49	125	256
1437093_at	Dnaic1	68922	0.49	161	327
1455604_at	Fzd5	14367	0.49	106	216
1454632_at	6330442E10Rik	268567	0.49	221	448
1439322_at			0.49	67	136
1451609_at	Tspan33	232670	0.49	147	299
1444137_at	A430108G06Rik	319650	0.49	39	80
1417829_a_at	Rab15	104886	0.49	486	985
1417643_at	Rsph1	22092	0.49	645	1307
1426261_s_at	Ugt1a1	22236	0.49	422	855
1423890_x_at	Atp1b1	11931	0.49	716	1448
1453836_a_at	Mgll	23945	0.49	196	396
1430157_at	1700095J03Rik	74293	0.49	29	59
1432083_a_at	Lrrc23	16977	0.50	453	915
1452913_at	Pcp4l1	66425	0.50	2495	5036
1428991_at	Hrasls	27281	0.50	93	188
1452904_at	1700026L06Rik	69987	0.50	358	721
1416966_at	Slc22a8	19879	0.50	47	94
1437580_s_at	Nek2	18005	0.50	240	483
1445532_at	Myo16	244281	0.50	128	257
1416203_at	Aqp1	11826	0.50	2668	5371
1437096_at	Ttc29	73301	0.50	91	184
1441867_x_at	4930534B04Rik	75216	0.50	203	407
1420918_at	Sgk3	170755	0.50	57	115
1434851_s_at	Crb3	224912	0.50	158	317

*Ratio >2-fold, average expression in at least one group >50, FDR<10%.

Table S3. Differentially* upregulated genes in *Gdf7-Cre/Otx2*$^{fl/fl}$ choroid plexus encoding secreted proteins (based on the GO term 'extracellular location')

Probe set	Gene symbol	Entrez	Linear fold change*	Average expression *Otx2* KO	Average expression WT
1420512_at	Dkk2	56811	6.87	2214	322
1460258_at	Lect1	16840	6.35	357	56
1422606_at	C1qtnf3	81799	5.63	444	79
1456084_x_at	Fmod	14264	4.82	2409	500
1449979_a_at	Spock3	72902	4.80	110	23
1455393_at	Cp	12870	4.61	502	109
1419383_at	S100b	20203	4.41	146	33
1460412_at	Fbln7	70370	4.25	199	47
1434779_at	Cbln2	12405	3.79	385	102
1418486_at	Vnn1	22361	3.42	211	62
1433532_a_at	Mbp	17196	3.22	152	47
1449465_at	Reln	19699	3.19	1878	588
1425039_at	Itgbl1	223272	3.09	67	22
1416371_at	Apod	11815	3.01	1016	338
1449254_at	Spp1	20750	2.99	641	214
1449319_at	Rspo1	192199	2.99	481	161
1450728_at	Fjx1	14221	2.90	647	223
1441693_at	Adamts3	330119	2.90	479	165
1433529_at	Pamr1	210622	2.88	189	66
1425425_a_at	Wif1	24117	2.64	312	118
1429459_at	Sema3d	108151	2.61	113	43
1419717_at	Sema3e	20349	2.60	366	141
1449368_at	Dcn	13179	2.49	2743	1100
1437218_at	Fn1	14268	2.49	114	46
1415935_at	Smoc2	64074	2.33	204	87
1452968_at	Cthrc1	68588	2.30	1528	665
1430700_a_at	Pla2g7	27226	2.27	884	390
1448228_at	Lox	16948	2.26	406	180
1448598_at	Mmp17	23948	2.19	194	89
1439827_at	Adamts12	239337	2.18	995	456
1420484_a_at	Vtn	22370	2.17	791	364
1425575_at	Epha3	13837	2.16	316	146
1453084_s_at	Col22a1	69700	2.16	600	278
1448823_at	Cxcl12	20315	2.16	973	451
1438020_at	Hapln1	12950	2.16	95	44
1447839_x_at	Adm	11535	2.15	88	41
1423407_a_at	Fbln2	14115	2.15	936	435
1433653_at	Fam20a	208659	2.13	102	48
1417455_at	Tgfb3	21809	2.11	745	352
1430352_at	Adamts9	101401	2.11	60	28
1416625_at	Serping1	12258	2.10	644	306
1450085_at	Angptl2	26360	2.10	376	179
1450782_at	Wnt4	22417	2.07	737	356
1418376_at	Fgf15	14170	2.06	523	254
1423250_a_at	Tgfb2	21808	2.05	419	204

1448201	at	Sfrp2	20319	2.05	1420	692
1436755	at	Itih5	209378	2.04	109	54
1448929	at	Fl3a1	74145	2.03	1725	848
1433428	x at	Tgm2	21817	2.03	480	236
1422831	at	Fbn2	14119	2.03	1348	665

*Ratio >2-fold, average expression in at least one group >50, FDR<l0%.

Table S4. Differentially* downregulated genes in *Gdf7-Cre/Otx2*$^{fl/fl}$ choroid plexus encoding secreted proteins (based on the GO term 'extracellular location')

Probe set	Gene symbol	Entrez	Linear fold change*	Average expression *Otx2* KO	Average expression WT
1429361_at	Pmch	110312	0.11	115	1011
1418190_at	Pon1	18979	0.23	30	126
1418440_at	Col8a1	12837	0.24	197	812
1434719_at	A2m	232345	0.27	571	2117
1427038_at	Penk	18619	0.30	1567	5311
1420763_at	Klk4	56640	0.30	143	473
1429348_at	Sema3c	20348	0.31	753	2428
1421429_a_at	Npnt	114249	0.34	124	363
1427775_at	Defb10	246085	0.35	175	506
1452277_at	Arsg	74008	0.35	265	748
1436127_at	Crhbp	12919	0.35	45	127
1419139_at	Gdf5	14563	0.39	206	533
1440250_at	Col4a4	12829	0.39	47	121
1438779_at	Col4a3	12828	0.40	64	162
1438200_at	Sulf1	240725	0.43	1735	4047
1449340_at	Sostdc1	66042	0.43	1808	4209
1428811_at	Wfikkn2	278507	0.45	652	1448
1460734_at	Col9a3	12841	0.45	1363	3020
1436474_at	Clec18a	353287	0.45	52	114
1451527_at	Pcolce2	76477	0.45	213	472
1453152_at	Mamdc2	71738	0.46	161	353
1456741_s_at	Gpm6a	234267	0.47	772	1650
1421844_at	Il1rap	16180	0.49	104	213
1437094_x_at	Dnaic1	68922	0.49	213	437

*Ratio >2-fold, average expression in at least one group >50, FDR<10%.

Table S5. Primers used in real-time PCR

Gene	Forward primer (5′-3′)	Reverse primer (5′-3′)
Axin2	AGCGCCAACGACAGCGAGTT	CAGGCGGTGGGTTCTCGGAAA
Calb2	TTGAGATGGCGGAGCTGGCG	AGGTTCATCATAGGGCCTGTTGGC
Cdkn1a	CCAGACATTCAGAGCCACAGGCAC	GCATCGCAATCACGGCGCAA
c-Myc	ACCACCAGCAGCGACTCTGAAGA	GGGTGCGGCGTAGTTGTGCT
Dkk2	CAGCTCGCGGGCCAAACTCA	AGGCCTGCCCCAGGCTTTTG
Etv4	GGACCAGCGAGTGCCCTACA	TCCGGTACCTGAGCTTCTGCG
Etv5	ACCGGAAGAGGTTGCTCGCC	GGGCGCTGATTGTCCGGGAA
Fgf15	GGTCGCTCTGAAGACGATTGCC	TCCTCCGAGTAGCGAATCAGCC
Fzd5	CCCAGCAGGATCCTCCGAGAGTT	CGGGCTGGCAACCTGTTGGT
Gapdh	ATTCAACGGCACAGTCAAGG	TGGATGCAGGGATGATGTTC
Gfap	AGCCCTGGACATCGAGATCGCC	CTTTGGTGCTTTTGCCCCCTCGGA
Gli1	TGGAGGTCTGCGTGGTAGA	TTGAACATGGCGTCTCAGG
Gli3	TCGGCAAGTGCAATCAGCCCTG	AGGGCTGTGTCCGAATGCGG
Hes1	TGCCAGCTGATATAATGGAGAA	CCATGATAGGCTTTGATGACTTT
Hes5	AGTCCTGGTGCAGGCTCTT	CAGCCCAACTCCAAGCTG
Ngn2	ACCGCATGCACAACCTAAAC	AGCGCCCAGATGTAATTGTG
Otx2	GGGCACAGCTCGACGTTCTGG	AACCATACCTGCACCCTGGATTCT
Penk	CGCGGTTCCTGAGGCTTTGC	TGCACGCCAGGAAATTGATGTCGC
Pmch	TTTGACATGCTCAGGTGTATGCTGGG	GCAACATCAAGGGCTTTTCTCCCCG
Reelin	AGAATGTGCCCCCGTTTGGC	TCCTTGTGCAGCTGTGTACCCC
Sfrp2	ACCTAGATGAGACCATCCAGCCG	ACACCTTGGGAGCTTCCTCTGTGGC
Shisa2	GACAGCTCGGCAGTCCCCAT	GTCTCCATCAGGCGGTTGGC
Wif	TTTACCTGGCAAGCTGCGGG	TGCCTTGTGAGGCACTGTTCCC